Isotopic constraints on the genesis and evolution of basanitic lavas at Haleakala, Island of Maui, Hawaii

Erin H. Phillips[a*], Kenneth W.W. Sims[a], David R. Sherrod[b], Vincent J.M. Salters[c], Jurek Blusztajn[d], Henrietta Dulai[e]

[a] *Department of Geology and Geophysics, University of Wyoming, Laramie, WY 82071, USA*
[b] *U.S. Geological Survey, Vancouver, WA 98683, USA*
[c] *National High Magnetic Field Laboratory, Department of Geological Sciences, Florida State University, Tallahassee, FL 32306, USA*
[d] *Department of Geology and Geophysics, Woods Hole Oceanographic Institution, Woods Hole, MA 02543, USA*
[e] *Department of Geology and Geophysics, University of Hawaii, Honolulu, HI 96822, USA*
** Corresponding author*

ABSTRACT

To understand the dynamics of solid mantle upwelling and melting in the Hawaiian plume, we present new major and trace element data, Nd, Sr, Hf, and Pb isotopic compositions, and ^{238}U-^{230}Th-^{226}Ra and ^{235}U-^{231}Pa-^{227}Ac activities for 13 Haleakala Crater nepheline normative basanites with ages ranging from ~900 to 4100 yr B.P.. These basanites of the Hana Volcanics exhibit an enrichment in incompatible trace elements and a more depleted isotopic signature than similarly aged Hawaiian shield lavas from Kilauea and Mauna Loa. Here we posit that as the Pacific lithosphere beneath the active shield volcanoes moves away from the center of the Hawaiian plume, increased incorporation of an intrinsic depleted component with relatively low $^{206}Pb/^{204}Pb$ produces the source of the basanites of the Hana Volcanics. Haleakala Crater basanites have average ($^{230}Th/^{238}U$) of 1.23 (n=13), average age-corrected ($^{226}Ra/^{230}Th$) of 1.25 (n=13), and average ($^{231}Pa/^{235}U$) of 1.67 (n=4), significantly higher than Kilauea and Mauna Loa tholeiites. U-series modeling shows that solid mantle upwelling velocity for Haleakala Crater basanites ranges from ~0.7 to 1.0 cm/yr, compared to ~10 to 20 cm/yr for tholeiites and ~1 to 2 cm/yr for alkali basalts. These modeling results indicate that solid mantle upwelling rates and porosity of the melting zone are lower for Hana Volcanics basanites than for shield-stage tholeiites from Kilauea and Mauna Loa and alkali basalts from Hualalai. The melting rate, which is directly proportional to both the solid mantle upwelling rate and the degree of melting, is therefore greatest in the center of the Hawaiian plume and lower on its periphery. Our results indicate that solid mantle upwelling velocity is at least 10 times higher at the center of the plume than at its periphery under Haleakala.

1. INTRODUCTION

In order to interpret the dynamics and structure of the Hawaiian plume, it is necessary to consider not only the predominant and well-studied shield-stage tholeiitic volcanism, but also late-stage alkaline volcanism. These silica-undersaturated lavas tap magma from the periphery of the plume as the Pacific lithosphere beneath the active shield volcanoes moves away from the plume center.

Shield-stage volcanism in Hawaii has been widely studied since the work of the pioneering geologists H. T. Stearns and G. A. Macdonald in the 1940s. Haleakala, which is located on the island of Maui approximately 240 km to the northwest of the inferred center of the hotspot (DePaolo and Stolper, 1996; Fig. 1), presents an opportunity to study alkaline volcanism on the trailing edge of the Hawaiian plume. The youngest (<0.15-0.12 Ma) alkaline lavas from Haleakala are the Hana Volcanics, which have been classified as rejuvenated stage volcanism (Bergmanis et al., 2000; Stearns and Macdonald, 1942). This assertion, however, has been challenged by Sherrod et al. (2003) based on the lack of a significant volcanic hiatus prior to eruption of the Hana Volcanics and the geochemical similarity of the upper Kula and Hana Volcanics. Regardless of their classification as either postshield stage or rejuvenated stage volcanism, the youngest Haleakala lavas are highly alkaline, silica-undersaturated basanites from the periphery of the Hawaiian plume. In this study, we will refer to these lavas as postshield stage, consistent with Sherrod et al. (2003).

Here we examine a suite of 13 young basanitic lavas from Haleakala Crater using U-series, Nd, Sr, Hf, and Pb isotopes, and major- and trace-element abundances. These silica-undersaturated basanites are ideal samples to study waning volcanism at the Hawaiian hotspot as the Pacific plate moves to the northwest at a rate of 9-10 cm/yr (Clague and Dalrymple, 1987). As such, these late-stage lavas provide clues on the structure and geodynamical processes of the Hawaiian plume, the mantle sources of alkaline lavas, and the processes that occur during melting and magma transport. By comparing the major and trace element concentrations and isotope compositions of known-age Haleakala basanites to young, similarly aged shield-stage tholeiites from Kilauea and Mauna Loa and alkali basalts from Hualalai and Mauna Kea, we are able to draw conclusions about the Hawaiian plume as a whole.

U-series isotopes (^{238}U-^{230}Th-^{226}Ra and ^{235}U-^{231}Pa) are especially useful in elucidating the time scales of melting processes because the half-lives of ^{230}Th (75.4 kyr), ^{226}Ra (1.6 kyr), and ^{231}Pa (32.8 kyr) are on the same order as the time scales of melt generation and extraction. The small solid/liquid partition coefficients of U, Th,

Ra, and Pa make it possible to glean information about the porosity of the melting zone and the rate of mantle upwelling (e.g., Beattie, 1993; Elkins et al., 2008; LaTourrette et al., 1993; Salters and Longhi, 1999; Sims et al., 1999).

The source of Hawaiian lavas and the possible presence of a mafic component in the mantle beneath Hawaii are topics of considerable debate. Some studies have implied that partial melting of subducted oceanic plates, combined with mantle peridotite, play a role in the generation of Hawaiian lavas (e.g., Hauri, 1996; Sobolev et al., 2005), while others suggest that peridotite melting alone can produce the geochemical signatures observed (e.g., Elkins et al., 2008; Sims et al., 1995, 1999; Stracke et al., 1999). Additionally, a characteristic of late-stage alkaline lavas in Hawaii, such as Haleakala Crater basanites, is their depleted Nd, Sr, and Hf isotope signatures that accompany enrichment in incompatible trace elements (e.g., Chen and Frey, 1983; 1985). The origin of the depleted signature is debated (e.g., Bizimis et al., 2013; Blichert-Toft et al., 1999; Chen and Frey, 1985; Cousens and Clague, 2015; Dixon et al., 2008; Frey et al., 2005; Garcia et al., 2010; West and Leeman, 1987; Xu et al., 2005). Our new long-lived radioisotope data for Haleakala Crater basanites answer questions regarding the mantle source of Hawaiian lavas and, when combined with U-series isotopic data and major and trace element geochemical data, provide a mapping of the upwelling structure of the Hawaiian plume.

2. GEOLOGIC BACKGROUND

Hawaii is considered by many to be the quintessential example of hotspot volcanism. Early work by J.T. Wilson and W.J. Morgan laid out a framework for understanding hotspot volcanism in the context of mantle plumes (e.g., Morgan, 1971; Wilson, 1963). Three lines of evidence that support the existence of stationary mantle upwellings beneath moving lithospheric plates are: (1) well-documented observations of age progressive island chains, typified by the Hawaiian-Emperor islands and seamounts (Wilson, 1963); (2) seismic imaging of low velocity zones at

depth (e.g., Wolfe et al., 2011; Zhao et al., 2013); and (3) geochemical models (Bourdon and Sims, 2003; Pietruszka et al., 2001; Sims et al., 1999) and fluid mechanical models (Hauri et al., 1994; Ribe and Christensen, 1999; Watson and McKenzie, 1991) that reveal rapidly upwelling cores and more slowly upwelling peripheries.

The evolution of Hawaiian volcanoes comprises four stages, as recognized by Stearns (1940) and described in detail by Clague (1987). Pre-shield stage volcanism consists of basanite, alkali basalt, transitional basalt, and tholeiite. During the tholeiitic shield-building stage, currently typified by Kilauea and Mauna Loa , >95% of the volume of a given volcano is erupted. Ensuing postshield stage volcanism consists primarily of hawaiite, mugearite, benmoreite, and alkali basalt. The rejuvenated stage, also referred to as post-erosional in early literature, is characterized by eruption of alkali basalt and basanite and occurs after a period of quiescence, up to ~2 m.y. after completion of the postshield stage (Clague and Sherrod, 2014). Although numerous contributions have focused on older postshield and rejuvenated lavas (e.g., Dixon et al., 2008; Garcia et al., 2010) and shield-stage lavas (e.g., Gaffney et al., 2004; Huang et al., 2005; Jackson et al., 2012; Nobra Silva et al., 2013; Ren et al., 2006, 2009; Weis et al., 2011), here our focus is on young known-age Hawaiian lavas. Specifically we compare postshield basanites from Haleakala with similarly aged (<6000 yr B.P.) tholeiites from Kilauea and Mauna Loa and alkali basalts from Mauna Kea and Hualalai.

A detailed description of the petrology and geochemistry of Haleakala lavas is presented by Macdonald and Powers (1968) and a general description of the geology of Haleakala is given by Macdonald and Abbott (1970). Pre-shield stage lavas from Haleakala are buried (Sherrod et al., 2003). The overlying lavas are divided into three units. The Honomanu Basalt represents the shield-building stage and consists predominantly of tholeiites. Its lavas are older than ~0.93 Ma (Chen et al., 1991). The postshield Kula Volcanics unit consists mostly of alkali basalt and hawaiite, with rare mugearite and ankaramite (Chen et al., 1990). These lavas

erupted between 0.93 Ma and 0.13-0.14 Ma (Chen et al., 1991; Coe et al., 2004; Sherrod et al., 2003). The youngest unit at Haleakala is the Hana Volcanics (Bergmanis et al., 2000; Sherrod et al., 2003), which is younger than 0.15-0.12 Ma (Sherrod et al., 2003; Fig. 1). The Hana Volcanics unit is predominantly basanite with scant alkali basalt. As previously stated, we refer here to the Hana Volcanics as postshield stage lavas, following the interpretation of Sherrod et al. (2003), but emphasize that regardless of the classification of their eruptive stage, these lavas are highly alkaline and erupted much farther from the plume center than shield-stage Hawaiian tholeiites. West and Leeman (1987) note that there is no signficant difference in the Pb or Sr isotopic composition between the Kula and Hana lavas, consistent with the interpretation of Sherrod et al. (2003) that both units are postshield lavas. The designation of eruptive stage has significance for hazard analysis due to the difference in overall volume of erupted products between postshield and rejuvenated stage volcanism, as well as the timing of an eruptive hiatus. The youngest lava flows on Haleakala are the Keonehunehune and Kalua o Lapa flows. The Kalua o Lapa flow was previously thought to have erupted in the mid to late 1700s (Oostdam, 1965; Stearns and Macdonald, 1942;), but Sherrod et al. (2006) revised the combined age range of the Keonehunehune and Kalua o Lapa flows to 330-460 ^{14}C yr B.P.

3. SAMPLES

In this study we have analyzed 13 new basanite samples from Haleakala Crater, all younger than ~4100 yr B.P. (Fig. 1; Table 1). Seven of these samples have radiocarbon ages that range from 870±40 yr to 4070±50 yr B.P. (Sherrod and McGeehin, 1999). The ages of the other six are bracketed by stratigraphic relations with dated lava flows, the extent of weathering and soil development, and paleomagnetic directions in conjunction with the paleosecular variation curve, and range from approximately 900 to 4000 yr B.P. (Sherrod et al., 2006). Knowledge of the ages of these samples is important for the interpretation of their U-series disequilibria.

158
159 In previous studies by Sims et al. (1995; 1999), ^{238}U-^{230}Th-^{226}Ra and ^{235}U-^{231}Pa
160 disequilibria, and Sr and Nd isotope data for five samples from the southwest rift
161 zone (SWRZ) of Haleakala were reported. Hafnium isotopic data for the SWRZ
162 samples are from Stracke et al. (1999) and we present Pb data for these five samples
163 in Table 3. SWRZ and Haleakala Crater lavas are all part of the Hana Volcanics and
164 are of similar age and composition. Because of their similarity, the SWRZ samples
165 and the new Haleakala Crater samples will be grouped together and referred to as
166 the Hana Volcanics in the subsequent text.
167
168 **4. ANALYTICAL METHODS**
169
170 Prior to analyses, phenocryst phases (primarily olivine, clinopyroxene, and
171 plagioclase) were removed from rock chips by hand picking. Therefore, analyses are
172 for groundmass only, which eliminates complications presented by possible
173 xenocrystic material or shallow fractional crystallization. Major and trace element
174 concentrations were measured at Boston University by inductively coupled plasma
175 optical emission spectrometry (ICP-OES) and inductively coupled plasma mass
176 spectrometry (ICP-MS), respectively. See Table 2 for details on analytical precision
177 and analyses of rock standards.
178
179 Strontium, Nd, and Pb isotopes were measured at Woods Hole Oceanographic
180 Institution (WHOI) with a Thermo Fisher Neptune multi-collector inductively
181 coupled plasma mass spectrometer (MC-ICP-MS). Samples were picked free of
182 alteration and leached in sequential batches of deionized water, 0.1M oxalic acid +
183 2% H_2O_2, 0.1M HCl + 2% H_2O_2, and deionized water. For Sr and Nd separation,
184 powders were dissolved in concentrated HF and $HClO_4$, followed by three dry
185 downs in 6.2N HCl to convert fluorides to chlorides. Separation of Sr and Nd was
186 carried out by conventional ion-exchange chromatography using DOWEX 50 cation-
187 exchange resin and then HDEHP-coated Teflon powder (Taras and Hart, 1987). Lead
188 was separated following the HBr-HNO_3 procedure of Abouchami et al. (1999) using
189 a single column pass. Hafnium isotopes were analyzed using the Lamont Isolab 54

Secondary Ionization mass spectrometer (England et al., 1992) at the National High Magnetic Field Laboratory (see Salters et al., 2010). The Hf fraction was separated using the technique described by Munker et al. (2001). See Table 3 and Hart and Blusztajn (2006), Hart et al. (2004; 2005), Munker et al. (2001) and Sims et al. (2008a) for further analytical details.

U-Th isotopic compositions were measured with a Thermo Fisher Neptune MC-ICP-MS at WHOI. Thorium and U were separated and purified at WHOI using two anion columns. Separate liquid aliquots of the same dissolution were used to measure U and Th concentrations. Concentrations were measured by isotope dilution using a Thermo Fisher Element 2 high resolution sector-field ICP-MS at WHOI, with a peak jumping routine. Samples were spiked with ^{229}Th and ^{233}U and equilibrated to attain ^{232}Th/^{229}Th ≈ 30 and ^{238}U/^{233}U ≈ 10. Further analytical details can be found in Table 4 and Ball et al. (2008), and Sims et al. (2008b; 2008c).

The ^{226}Ra concentrations were analyzed by isotope dilution mass spectrometry at WHOI with a Thermo Fisher Neptune MC-ICP-MS on separate aliquots from the same rock dissolution. See Sims et al. (2008c) for complete details on the separation and purification of Ra and additional analytical methods. ^{231}Pa concentrations were measured by isotope dilution on a Thermo Fisher Element 2 ICP-MS at WHOI. See Choi et al. (2001), Pichat et al. (2004), Sims et al. (1999), Sims et al. (2002), and Sims et al. (2008c) for further information about separation and purification of Pa and U-Pa methods. Actinium was separated by extraction chromatographic techniques and analyzed by alpha spectrometry at WHOI. See Dulaiova et al. (2013) for further details on separation and analysis of ^{227}Ac.

5. RESULTS

5.1. Major and trace element geochemistry

Haleakala Crater samples have SiO_2 ranging from 41.9 to 46.8 wt. % and K_2O+Na_2O between 3.4 and 7.0 wt. % (Table 2). Haleakala Crater and SWRZ basanites have lower SiO_2, higher Na_2O+K_2O and are enriched in highly incompatible elements

relative to shield-stage tholeiitic basalt erupted at the currently active Kilauea and Mauna Loa volcanoes (Figs. 2 and 3; Table 2). Haleakala lavas are also compared to Mauna Kea and Hualalai lavas, which include alkali basalts, hawaiites and mugearites and Loihi lavas, which are a combination of tholeiites and alkali basalts. For completeness, data for Haleakala's shield-stage Honomanu Basalt, which is >0.93 Ma, are also included in selected figures. It is emphasized that our main goal is to compare Haleakala postshield lavas with similarly aged (<6000 yr B.P.) shield-stage lavas from Kilauea, Mauna Loa, Mauna Kea, and Hualalai, which are near the plume center. Haleakala's older shield-stage Honomanu Basalt is not considered representative of recent plume material.

5.2. Sr-Nd-Hf-Pb Isotope Results

Haleakala Crater samples have ε_{Nd} ranging from +7.3 to +8.5, which encompass the ε_{Nd} values of the SWRZ samples (Table 3; Sims et al., 1995; 1999). $^{87}Sr/^{86}Sr$ for the Hana Volcanics ranges from 0.70310 to 0.70333 (Table 3). Strontium isotopic compositions for three of the SWRZ samples are slightly lower than for the new crater samples, whereas the other two fall within the range of the crater samples (Sims et al., 1995; 1999). Haleakala Crater and SWRZ basanites have relatively low $^{87}Sr/^{86}Sr$ and high ε_{Nd} compared to shield-stage Hawaiian lavas (Fig. 4). ε_{Hf} for seven crater lavas (Table 3) and five SWRZ lavas (Stracke et al., 1999) ranges between +12.7 and +14.7. Consistent with the Nd and Sr isotopic data, ε_{Hf} values for the Hana Volcanics are higher than Hawaiian shield-stage lavas (Fig. 5).

The Hana Volcanics samples range in $^{206}Pb/^{204}Pb$ from 18.166 to 18.324, $^{207}Pb/^{204}Pb$ from 15.432 to 15.470, and $^{208}Pb/^{204}Pb$ from 37.699 to 37.907 (Table 3; Fig. 6). Within Hawaiian lavas, two trends in $^{206}Pb/^{204}Pb$ vs. $^{208}Pb/^{204}Pb$ space become apparent (Fig. 6a). Compositional heterogeneity in Hawaiian lavas is not only present in a temporal sense (i.e., pre-shield, shield, postshield, and rejuvenated stages), but also in a spatial sense, recognized as distinct geochemical differences between shield lavas of Kea trend volcanoes (including Mauna Kea, Kilauea, and Haleakala) and Loa trend volcanoes (including Mauna Loa, Loihi, and Hualalai;

Abouchami et al., 2005; Lassiter et al., 1996; Weis et al., 2011). The compilation of data in Figure 6a depicts the Kea and Loa trends, and shows that the basanites of the Hana Volcanics plot at the less radiogenic end of the Kea trend, when compared strictly with similarly aged Hawaiian lavas. It should be noted that older rejuvenated-stage lavas from East Molokai (~0.34-0.57 Ma; Xu et al., 2005) have Pb isotope compositions within the range of the Hana Volcanics. Some older rejuvenated-stage lavas from Niihau (Dixon et al., 2008) and Kauai (Garcia et al., 2010) also have Pb isotope compositions similar to the Hana Volcanics. In keeping with the aim of our study, we plot only data for relatively young lavas with ages similar to the Hana Volcanics.

5.3. U-series results

Basanites of the Hana Volcanics have ($^{230}Th/^{238}U$) from 1.18 to 1.32 for the 13 crater samples (Table 4) and 5 SWRZ samples (Sims et al., 1995; 1999), with an average ($^{230}Th/^{238}U$) of 1.24 (n=18). Age corrected ($^{226}Ra/^{230}Th$) is between 1.17 and 1.30 for the Hana Volcanics samples (Table 4 and Sims et al., 1995; 1999), with an average of 1.26 (n=18). ($^{231}Pa/^{235}U$) for four Haleakala Crater basanite samples (Table 4) and four SWRZ samples (Pickett and Murrell, 1997; Sims et al., 1995; 1999) ranges from 1.47 to 2.12, with an average of 1.70 (n=9). ($^{227}Ac/^{231}Pa$) was measured for four Haleakala Crater samples (Table 4). All four are in equilibrium, which is as expected for samples of this age (^{227}Ac $t_{1/2}$=21.8 yr). Sample HK-22 has ($^{231}Pa/^{235}U$) of 2.12, which is significantly higher than other Hana Volcanics samples. The equilibrium ($^{227}Ac/^{231}Pa$) for this sample demonstrates that this high Pa value is robust and lends credence to both the Pa and Ac methods. Additionally, this sample lies within the OIB field in ($^{230}Th/^{238}U$) versus ($^{231}Pa/^{235}U$) space (Lundstrom et al., 2003; Sims et al., 2008c), albeit at the high ($^{231}Pa/^{235}U$) end.

6. DISCUSSION

6.1 Mantle Sources of Postshield Haleakala Lavas

Late-stage alkaline Hawaiian lavas exhibit depleted isotopic signatures (relatively high ε_{Nd} and ε_{Hf} and low $^{87}Sr/^{86}Sr$) but are enriched in highly incompatible trace elements compared to shield-stage tholeiites (e.g., Bizimis et al., 2013; Chen and

Frey, 1983; 1985; Frey et al., 2005; Garcia et al., 2010; West and Leeman, 1987; Xu et al., 2005). This seemingly contradictory observation can be explained by small degrees of partial melting, which produces their characteristic basanitic compositions and light rare earth element enrichments (Fig. 3). Several papers have debated the origin of the depleted isotopic signature of alkaline Hawaiian lavas (e.g., Bryce et al., 2005; Frey et al., 2005; Lassiter et al., 1996; Xu et al., 2005). One question in this debate is whether the depleted signatures in postshield lavas are the result of mixing between the plume and the surrounding mantle or the result of intrinsic heterogeneities within the plume. Early studies proposed the depleted signatures were produced by increased mixing with a depleted mantle, or MORB-like, component as a volcanic center moved away from the center of the Hawaiian hotspot (e.g., Chen and Frey, 1985; West and Leeman, 1987). Chen and Frey (1985) argued that the enrichment of highly incompatible elements and the depleted Sr and Nd isotopic signatures in younger alkaline Haleakala lavas compared to older tholeiitic lavas requires a MORB component and a plume component. These authors conclude that the depleted isotopic signatures of these late-stage alkaline lavas are the result of decreased activity of the rising mantle plume and increased interaction between plume derived material and the surrounding wall rock toward the periphery of the plume. While the characteristic small degree of melting (F) of postshield Haleakala lavas is generally agreed upon, others argue that the long-lived depleted component observed in the isotopes is intrinsic to the Hawaiian plume (e.g., Bizimis et al., 2013; Fekiacova et al., 2007; Frey et al., 2005; Garcia et al., 2010). In particular, Frey et al. (2005) show that late-stage lavas are isotopically distinct from Pacific MORB in their Pb isotope ratios. Further, it is debated whether the isotopic heterogeneity of the Hawaiian plume originates in a deep thermal boundary layer and is vertically stretched on a large scale within the plume or the isotopic heterogeneity takes the form of fertile plums dispersed throughout a peridotite matrix (e.g., Abouchami et al., 2005; Hofmann and Farnetani, 2013).

Here we specifically focus on the mantle sources of the postshield lavas at Haleakala by comparing their trace element and isotopic characteristics to similarly aged

317 shield-stage lavas. Although deciphering the large-scale chemical and lithological
318 structure of the Hawaiian plume is beyond the scope of this paper, understanding
319 the mantle sources and melting processes of young postshield alkaline lavas can
320 provide perspective on the entirety of the Hawaiian plume. Indeed, in comparison
321 with other young Hawaiian lavas, the Hana Volcanics have higher ε_{Nd} and ε_{Hf} and
322 lower $^{87}Sr/^{86}Sr$ values, implying a greater contribution from a depleted source in
323 these postshield alkaline magmas (Figs. 4 and 5). Haleakala Crater basanites
324 analyzed in this study, as well as Haleakala SWRZ samples, plot closer to the high ε_{Nd}
325 and ε_{Hf} and low $^{87}Sr/^{86}Sr$ end of the array. These isotopic signatures are consistent
326 with increased involvement of a depleted component in late-stage alkaline magmas
327 as the lithosphere moves away from the center of the Hawaiian hotspot.
328
329 The Pb isotope ratios for the Hana Volcanics show more complicated relationships
330 with other young Hawaiian lavas (Fig. 6). As discussed in section 5.2, the Pb isotope
331 ratios of postshield Haleakala lavas are clearly within the spatial Kea trend
332 (Abouchami et al., 2005; Lassiter et al., 1996; Weis et al., 2011) and display non-
333 radiogenic Pb isotope compositions relative to other young Kea trend lavas plotted
334 in Figure 6a. It is again emphasized that the focus of our paper is to compare the
335 Hana Volcanics to similarly aged, young tholeiitic and alkali basalt lavas from near
336 the plume center.
337
338 The Hana Volcanics show a positive correlation between $^{87}Sr/^{86}Sr$ and $^{206}Pb/^{204}Pb$,
339 in contrast to the overall negative trend of Kilauea and Mauna Loa tholeiites (Fig.
340 6b). West and Leeman (1987) observed a similar trend for Haleakala postshield
341 lavas and concluded that two-component mixing is not a viable explanation for the
342 isotopic and geochemical characteristics of the different eruptive stages in Hawaii
343 and that a three (or more) component mixing model is required. They propose the
344 Hawaiian mantle plume is made up of primitive and enriched mantle components
345 that are mixed to variable degrees with a MORB-like component. We note, however,
346 that the positive trend for postshield lavas in Sr-Pb isotope space (Figure 6b) does

not point towards the average of the Pacific MORB field (e.g., 9-10°N EPR axial lavas; Sims et al., 2002), but could be explained by mixing with the enriched lavas of the Garrett Transform (Wendt et al., 1999). Xu et al. (2005) also discussed this negative trend in Sr-Pb isotope space for postshield lavas from Kea trend volcanoes and noted that they are influenced by a low $^{206}Pb/^{204}Pb$ and low $^{87}Sr/^{86}Sr$ component that clearly does not have a significant effect on the shield-stage lavas.

To model mixing between Hawaiian plume material and a MORB-like component, we have plotted Sr, Nd, and Pb isotopic ratios against the normalized Ce/Sm ratio. (Fig. 7). The utility of this comparison is that melting processes will affect the Ce/Sm ratio but not the isotope ratios. In this model, we assume Kilauea tholeiites, which along with Haleakala are part of the Kea trend, are representative of the most recent eruptive products from the center of the Hawaiian plume (Bryce et al. 2005; DePaolo and Stolper, 1996). Haleakala shield-stage lavas are much older (>0.9 Ma) and therefore are not considered representative of recent plume material. As illustrated in Figure 7 the Sr and Nd isotopes can be explained by melting a two-component mixture of Hawaiian plume material (represented by Kilauea tholeiites) and Pacific MORB. The $^{208}Pb/^{206}Pb$ data, however, do not support two-component mixing because both Pacific MORB and Hawaiian plume material have lower $^{208}Pb/^{206}Pb$ than Haleakala basanites. Varying the degree of melting or the partition coefficients does not change this relationship. It is permissible, however, that plume material mixed with either: (1) a high $^{208}Pb/^{206}Pb$ component (>2.10) similar to the enriched MORB from the Garrett Transform (Wendt et al., 1999); (2) the Depleted Rejuvenated Component (DRC) of Bizimis et al. (2013), proposed to explain the isotopic compositions of Kaula lavas and pyroxenite xenoliths; or (3) the Depleted Makapuu component (DMK) of Tanaka et al. (2002; 2008), proposed as the depleted end member for Koolau shield lavas. In any case, the Pb isotope data suggest that two-component mixing between plume material and Pacific MORB is not a viable explanation for the formation of the initial solid composition of the Haleakala postshield basanites; these data necessitate the involvement of a low $^{206}Pb/^{204}Pb$ (high $^{208}Pb/^{206}Pb$) component. We argue that the most logical conclusion is that this

low $^{87}Sr/^{86}Sr$, high $^{208}Pb/^{206}Pb$, and high $^{143}Nd/^{144}Nd$ component is an intrinsic part of the Hawaiian plume as suggested by numerous studies including Bizimis et al. (2013), Fekiacova et al. (2007), Frey et al. (2005), and Garcia et al. (2010).

This leads us to question the nature of this intrinsic component. While the heterogeneity of the mantle is well established, the extent to which this long-lived isotopic heterogeneity is the manifestation of lithological variability remains debated (e.g., Allègre and Turcotte, 1986; Donnelly et al., 2004; Hirschmann et al., 2003; Kogiso et al., 2003; Sims et al., 2013; Waters et al., 2011; Workman et al., 2004). At a given pressure, mafic lithologies (i.e., pyroxenites and eclogites) have lower solidus temperatures than peridotites, and the difference in temperature between the solidus and liquidus of pyroxenite is less than for peridotite. Pyroxenites thus produce more melt than peridotites and clearly their presence in the melting region can significantly affect the geochemistry of erupted lavas (e.g., Elkins et al., 2008, 2011, 2014; Hirschmann and Stolper, 1996; Hirschmann et al., 2003; Ito and Mahoney, 2005; Pertermann and Hirschmann, 1999; Prytulak and Elliott, 2009; Rudge et al., 2013; Sims et al., 2013; Stracke and Bourdon, 2009; Waters et al., 2011). As noted above, there are clearly multiple components in the source of Hawaiian lavas, indicated by long-lived radiogenic isotopes, and some studies provide strong evidence for the influence of pelagic sediments in the source of Hawaiian lavas (Blichert-Toft et al., 1999; Nielsen et al., 2006). Some research argues for lithological heterogeneity in the Hawaiian source (e.g., Bianco et al., 2005; Hauri, 1996; Jackson et al., 2012; Lassiter et al., 2000; Pietruszka et al., 2013), even including the argument that the Hawaiian source is olivine free (Sobolov et al., 2005). Others maintain that pyroxenite is not necessary to produce the geochemical signatures of Hawaiian lavas (e.g., Elkins et al., 2008; Marske et al., 2008; Matzen et al., 2013; Pietruszka et al., 2006; Salters et al., 2006; Sims et al., 1995; 1999; Stracke et al., 1999; Wagner and Grove, 1998; Wang and Gaetani, 2008).

U-Th-Ra and U-Pa disequilibria, coupled with other geochemical constraints, are potentially sensitive indicators of lithological variability in the mantle source (Elkins

et al., 2008; Prytulak and Elliott, 2009; Stracke et al., 2006; Stracke et al., 1999; Waters et al., 2011). In this context we use our U-Th-Ra and U-Pa data and major and trace element data to examine lithological heterogeneity in the Hawaiian plume source. Our new data from the Hana Volcanics are consistent with the conclusions of Stracke et al. (1999), who use Hf, Nd, and Th isotopes to argue that mafic lithologies are unlikely in the source of Hawaiian lavas. Stracke et al. (2006) point out that there is a wide range in the experimentally and theoretically determined values of the partition coefficients of U relative to Th (D_U/D_{Th}) in pyroxenitic and eclogitic sources (e.g., Pertermann and Hirschmann, 2002; Pertermann et al., 2004; van Westrenen et al., 1999) obfuscating the distinction between pyroxenitic and peridotitic melts. In contrast to these findings, more recent partitioning studies by Elkins et al. (2008) established that the partition coefficients for U and Th in garnet pyroxenites are significantly different than in peridotites. Differences in the fusibility of peridotites and pyroxenites can lead to significant differences in not only the U-series data but also in major and trace element compositions (Elkins et al., 2008, 2011, 2014; Prytulak and Elliott, 2009; Rudge et al. 2013; Sims et al., 2013; Waters et al., 2011).

As outlined below, our data clearly show that a mixed lithological source beneath Hawaii is not required to explain the U-series or other geochemical data for the Hana Volcanics. In fact, when using the pyroxenitic partition coefficients of Elkins et al. (2008), we do not see convergence in the modeled melting parameters for U-Th, U-Pa and Th-Ra disequilibria for the Hana Volcanics basanites (Table 5 and further discussed below in section 6.2). While some U-series studies demonstrate the need for pyroxenitic components in the source of MORB (e.g., Elkins et al., 2011; 2014; Waters et al., 2011), many OIB studies show that U-series data can be successfully modeled using a peridotitic source (e.g., Elkins et al., 2008; Prytulak and Elliott, 2009; Sims et al., 1999).

Select trace element ratios can potentially be indicative of the presence of recycled mafic components because of their contrasting solubilities and compatibilities in

residual phases during subduction (Kay, 1980; Pearce and Stern, 2006; Yogodzinski et al., 2015). The bulk partition coefficient for Ba in pyroxenite is an order of magnitude larger than in peridotite, whereas Ta is similar in both (Stracke and Bourdon, 2009), meaning that pyroxenitic lithologies retain Ba in their residual solids much more readily than peridotites. We posit that this partitioning difference in Ba/Ta, coupled with their respective behaviors during subduction will produce lower Ba/Ta ratios in erupted lavas containing a significant pyroxenitic component in their source. Isotopically depleted postshield lavas from Haleakala, including the Hana Volcanics, have high Ba/Ta ratios compared to most other young Hawaiian lavas (Fig. 8). The likelihood of a recycled mafic component in the source of Hana Volcanics is therefore less likely than in the source of Kilauea or Mauna Loa shield-stage tholeiites. It is noted that some trace element ratios such as Sr/Nd have also been used to discriminate between peridotitic and pyroxenitic sources. Small degrees of melting in Haleakala postshield lavas, evidenced by their enrichment in highly incompatible elements (Fig. 3), could have an overriding effect on trace element ratios such as Sr/Nd and mask the effect that source heterogeneity would have on these ratios. We therefore posit the Ba/Ta ratio as a good indicator of the higher likelihood of a pyroxenitic component in shield-stage lavas as opposed to postshield Haleakala lavas because of the combined effect of the traceable Ba/Ta composition of subducted oceanic crust and the difference in the Ba/Ta partition coefficients between peridotite and pyroxenite. If a pyroxenitic component is present in the Hawaiian plume, it is likely preferentially melted during the shield-stage, prior to eruption of postshield Haleakala lavas. Bizimis et al. (2013) also reached a similar conclusion in their study of rejuvenated lavas at Kaula. In addition to the Ba/Ta ratios, the depleted isotopic signature of Haleakala postshield lavas supports the argument against a pyroxenitic component in their source (Fig. 8). If derived from a recycled mafic component, the Haleakala postshield lavas would be expected to have a more enriched isotopic signature.

6.2 Solid mantle upwelling rates and buoyancy flux on the periphery of the Hawaiian plume

Because the half-life of ^{226}Ra (~1.6 kyr) is comparable to the estimated transport time for Hawaiian melts to rise through the melt column, ($^{226}Ra/^{230}Th$) data for Hawaiian basalts require models that consider the time-scales of melt generation and extraction. Dynamic melting (McKenzie, 1985) and chromatographic porous flow (Spiegelman and Elliott, 1993) are two end member fluid dynamical models invoked to explain U-series disequilibria. In dynamic melting, trapped melts remain in equilibrium with the solid until a critical porosity is attained, at which point melt in excess of this critical porosity is extracted from the melting region. In chromatographic porous flow, melt and solid maintain chemical equilibrium in the melt column and U-series disequilibria are the result of the more compatible parent nuclides travelling more slowly through the melt column than their respective daughter nuclides. The parent nuclides decay, leading to excesses of daughter nuclides, which are exemplified by ($^{230}Th/^{238}U$) and ($^{226}Ra/^{230}Th$) greater than 1 in many MORB and OIB basalts. Sims et al. (1999) investigated a limited suite of Hawaiian samples using ^{238}U-^{230}Th-^{226}Ra and ^{235}U-^{231}Pa disequilibria and found that both chromatographic porous flow (Spiegelman and Elliott, 1993) and dynamic melting (McKenzie, 1985) models can explain the observed data and suggest that solid mantle upwelling rate and maximum porosity of the melting zone are greater for tholeiites than for alkali basalts and basanites and that solid mantle upwelling velocity decreases with distance from the center of the Hawaiian plume, consistent with the geodynamical models of Hauri et al. (1994), Ribe and Christensen (1999), and Watson and McKenzie (1991).

The Haleakala Crater data presented here are consistent with those of Sims et al. (1995; 1999); namely, they exhibit higher ($^{230}Th/^{238}U$), ($^{226}Ra/^{230}Th$), and ($^{231}Pa/^{235}U$) disequilibria values than Hawaiian tholeiites and alkali basalts. ^{230}Th excesses indicate melting of a source containing residual garnet. Dynamic melting models, in combination with Ra and Th disequilibria, suggest melting rates between $1x10^{-5}$ and $1x10^{-4}$ kg $m^{-3}yr^{-1}$ with melt zone porosities between 0.2% and 0.5% for Haleakala basanites (Fig. 9). Some Pa disequilibria data lie outside the dynamic melting model grid shown in Figure 9 but are generally consistent with these

conclusions. These melting rates and porosities for Haleakala basanites are lower than those for shield-stage tholeiites from Kilauea and Mauna Loa, which are greater than $2x10^{-4}$ kg $m^{-3}yr^{-1}$ and between about 0.2% and 2%, respectively.

In dynamic melting models, the melt extraction velocity cannot be calculated explicitly and the melt transport time is assumed to be very short compared to the half-life of the shortest-lived daughter (^{226}Ra; $t_{1/2}$~1.6 kyr), whereas in the chromatographic porous flow model melt extraction velocity relative to solid mantle upwelling is calculated explicitly (e.g., Sims et al., 1999; Spiegelman and Elliott, 1993). The importance of melt transport time has been highlighted in several studies including Sims et al. (2002) for EMORB from the East Pacific Rise, Stracke et al. (2006) for Icelandic basalts from Theistareykir, and Weatherly and Katz (2016) for MORB.

At Hawaii, however, data for young basalts presented here and in Sims et al. (1995; 1999) can be successfully modeled with dynamic melting by varying only the porosity and solid mantle upwelling velocity. As a first order constraint, it is clear that ^{226}Ra excesses require melt transport times much less than 8,000 years (i.e., < five half-lives of ^{226}Ra). While we cannot argue against transport times on the order of <1 kyr for the Hana Volcanics, there is no indication in the data that such a correction is necessary. Some OIBs, such as young lavas (<300 yr B.P.) from the Canary Islands, have higher Ra excesses than the Hana Volcanics (($^{226}Ra/^{230}Th$) up to 1.8; Lundstrom et al., 2003), but they also have overall higher ^{231}Pa excess (($^{231}Pa/^{235}U$) up to 2.0). Melt transport on these timescales would not have an appreciable effect on ($^{231}Pa/^{238}U$) disequilibria because the half-life of ^{231}Pa is ~32.8 kyr. Therefore, in the absence of further evidence that melt transport time was appreciable relative to the half-life of ^{226}Ra, we do not further consider it in our dynamic melting models. Additionally, if melt transport was long enough to appreciably affect $^{226}Ra/^{230}Th$ disequilibrium, the initial ^{226}Ra excesses would have been even larger than those measured, requiring even lower porosities. In any case, solid mantle upwelling rate would be little affected because variations in this

parameter are mostly associated with (^{230}Th/^{238}U) disequilibria. As highlighted in previous studies (e.g., Sims et al., 1999, 2002; Stracke et al., 2006) uncertainties in partition coefficients are significant and are the limiting factor in these calculations.

Chromatographic modeling results (using the UserCalc program of Spiegelman, 2000) imply maximum porosity of the melt zone of ~0.5-0.6% for tholeiites, ~0.2-0.3% for alkali basalts, and ~0.1-0.3% for basanites and modeled solid mantle upwelling velocities of ~10-20 cm/yr for tholeiites, ~1-2 cm/yr for alkali basalts, and ~0.7-1.0 cm/yr for basanites (Fig. 10). In Figure 10, uncertainties on the average disequilibria values shown are signified with one standard deviation error envelopes. For pre-shield volcanism at Loihi, Sims et al. (1999) model the solid mantle upwelling velocity of Loihi tholeiites to be between ~15 and 35 cm/yr and alkali basalts between ~8 and 10 cm/yr based on (^{230}Th/^{238}U) and (^{231}Pa/^{235}U) disequilibria. Pietruszka et al. (2011) model upwelling rates at Loihi of ~5-6 cm/yr, utilizing their (^{230}Th/^{238}U) data and (^{226}Ra/^{230}Th) data of Rubin et al. (2005).

The following equations display the relationships between the critical parameters considered in the chromatographic porous flow model (see Spiegelman and Elliott, 1993 and Appendix 1 in Sims et al., 1999).

$$w = \frac{\Gamma d}{\rho_l \phi 2} \qquad (1)$$

where w is the average melt velocity, Γ is the melting rate, d is the length of the melt column, ρ_l is the density of the melt, and ϕ is the porosity. The melting rate is defined as:

$$\Gamma = \frac{W \rho_s F_{max}}{d} \qquad (2)$$

where W is the solid upwelling velocity and F_{max} is the maximum melt fraction. These equations serve to demonstrate that the melting rate is directly proportional to both the solid upwelling rate (W) and the degree of melting (F_{max}/d). As previously shown, Haleakala postshield basanites exhibit higher (^{230}Th/^{238}U) than other young Hawaiian lavas. (^{230}Th/^{238}U) is correlated with other trace element

562 ratios, including Sm/Nd as represented by $\alpha_{Sm/Nd}$ (Fig. 11), where $\alpha_{Sm/Nd}$ represents
563 Sm/Nd fractionation and is defined as $(Sm/Nd)_{magma}/(Sm/Nd)_{source}$. Lavas of the
564 Hana Volcanics show a greater degree of Sm/Nd fractionation than Hawaiian
565 tholeiites and alkali basalts, demonstrating that ($^{230}Th/^{238}U$) and Sm/Nd
566 fractionation vary with composition and this variability in trace element ratio
567 fractionation and major element composition can be attributed to varying degrees
568 of partial melting (Sims et al., 1995; 1999). We emphasize that the basanitic
569 composition (high Na_2O+K_2O) and enrichment in highly incompatible trace
570 elements require that the Haleakala postshield lavas are the result of small degrees
571 of partial melting. The correlation between U/Th fractionation, Sm/Nd
572 fractionation, and major element indices, including $Na_{8.0}$ and the silica saturation
573 index, in Hawaiian data is parameterized by Sims et al. (1995). In the buoyant
574 Hawaiian plume, elemental U/Th fractionation plays an important role in generating
575 ($^{230}Th/^{238}U$) disequilibrium, whereas in less buoyant plumes ^{230}Th ingrowth is more
576 significant (Elliott, 1997; Sims and Hart, 2006; Sims et al., 1995; 1999). In this
577 regard, we note that the lower upwelling rate at the plume edge increases the
578 amount of ingrown ^{230}Th, but the postshield basanitic lavas from Haleakala are also
579 lower degree melts than the shield-stage tholeiites, and so we argue that both of
580 these factors are influencing the large ^{230}Th excesses in the Haleakala basanites. As
581 indicated by equation (2) above, the small degrees of partial melting of the
582 Haleakala basanites coupled with low melting rates, produce high ($^{230}Th/^{238}U$)
583 disequilibria. Our models show that the solid mantle upwelling rates for Haleakala
584 postshield lavas are at least 10 times lower than for shield-stage tholeiites from
585 Kilauea and Mauna Loa.
586
587 In this modeling context we note that utilization of D values for a garnet pyroxenite
588 source from Elkins et al. (2008) did not converge on a unique solution for Haleakala
589 basanites or Hualalai alkali basalts in chromatographic porous flow models (Table
590 5). For Kilauea and Mauna Loa tholeiites, the upper end of the range of D values for
591 garnet pyroxenites from Elkins et al. (2008) resulted in no model convergence,
592 whereas the lower end of the range resulted in modeled solid mantle upwelling

593 velocity of 90-200 cm/yr and porosity of 5-7%. As discussed in the previous section,
594 the range in D values for U and Th in mafic lithologies complicates using U-series
595 disequilibria to definitively discriminate between peridotitic, pyroxenitic, and
596 eclogitic sources (Stracke et al., 2006). Although some variation is apparent in the
597 modeled porosity and solid mantle upwelling velocity based on different D values
598 for garnet peridotite sources (Table 5), there is a robust difference between the
599 solid mantle upwelling rates and porosities for shield-stage tholeiites from Kilauea
600 and Mauna Loa and the postshield basanites from Haleakala.
601
602 Because (^{230}Th/^{238}U), (^{226}Ra/^{230}Th), and (^{231}Pa/^{235}U) disequilibrium is partially a
603 function of mantle upwelling rate (equation 2 above), the buoyancy flux (B) of a
604 mantle plume can be calculated from the following expression (Bourdon et al., 1998;
605 Bourdon and Sims, 2003):
606 $$B = (8\pi\mu/g)*W^2 \qquad (3)$$
607 where μ is the viscosity and W is the upwelling rate. The buoyancy flux for a plume
608 of entirely thermal origin as defined by Sleep (1990) and discussed by Chabaux and
609 Allègre (1994) is:
610 $$B = \rho_m \propto \Delta T Q_p \qquad (4)$$
611 where ρ_m is the density of the mantle (3300 kg/m^3), α is the thermal expansion
612 coefficient ($3x10^{-5}$ °C^{-1}), ΔT is the excess temperature of the plume, and Q_p is the
613 volume flux of the plume. Chabaux and Allègre (1994) demonstrate an inverse
614 relationship between (^{230}Th/^{238}U) disequilibria and buoyancy flux. Bourdon et al.
615 (2006) suggest a similar inverse relationship between (^{231}Pa/^{235}U) disequilibria and
616 buoyancy flux.
617
618 The buoyancy flux of the Hawaiian swell, or the topographic anomaly related to the
619 hotspot, is estimated by Sleep (1990) as 8.7 Mg/s. Based on three-dimensional
620 numerical modeling, Ribe and Christensen (1994) propose that the buoyancy flux of
621 the Hawaiian plume itself is 4.1 Mg/s. Ribe and Christensen (1999) further refine

622 this estimate by taking into account both the thermal buoyancy flux and the
623 depletion buoyancy flux to arrive at a total buoyancy flux of 4.0 Mg/s.
624
625 We note that buoyancy flux estimates do not take into consideration differences in
626 upwelling rates between the center of the plume and its periphery. Using the U-
627 series data presented here for postshield lavas at Haleakala and the relationships
628 between U-series disequilibria and buoyancy flux presented in Bourdon et al.
629 (2006), we estimate the buoyancy flux at the trailing edge of the Hawaiian plume.
630 Using the average Hana Volcanics ($^{230}Th/^{238}U$) of 1.24 (n=18; 0.045 1σ std dev), the
631 average ($^{231}Pa/^{235}U$) of 1.70 (n=9; 0.190 1σ std dev), and assuming a viscosity of
632 $5x10^{20}$ Pa s, a buoyancy flux of ~1.5 Mg/s is inferred based on ($^{230}Th/^{238}U$) and ~2.2
633 Mg/s based on ($^{231}Pa/^{235}U$). Bourdon et al. (2006) also model buoyancy flux based
634 on excess temperature and predict the excess temperature at the top of the
635 Hawaiian plume to be 200°C. Putirka (2008) estimates the excess temperature of
636 the Hawaiian plume as 290°C. Assuming an excess temperature between 200°C and
637 300°C, a buoyancy flux of ~1.5-2.2 Mg/s is inferred from both ($^{230}Th/^{238}U$) and
638 ($^{231}Pa/^{235}U$) (see Fig. 4 in Bourdon et al., 2006). In summary, the buoyancy flux of
639 the postshield Haleakala lavas deduced from our U-series isotope data and the
640 models of Bourdon et al. (2006) is between ~1.5 and 2.2 Mg/s. Clearly there are
641 large uncertainties associated with the parameters discussed here, but this
642 buoyancy flux estimate for the periphery of the Hawaiian plume is approximately
643 one half of the buoyancy flux value of 4.1 Mg/s for the plume as a whole calculated
644 by Ribe and Christensen (1994). Undoubtedly the buoyancy flux is greatest at the
645 center of the plume; however, it is necessary to integrate the buoyancy flux over the
646 whole of a mantle plume, including the slower upwelling periphery, in order to
647 arrive at a reliable estimate for overall buoyancy flux.
648
649
650 **6.3 An updated model for the dynamics of the Hawaiian plume**
651 The preceding discussion leads to the following observations and inferences
652 regarding Haleakala postshield lavas and their relation to young shield-stage lavas
653 from the plume center: (1) Relative to young Hawaiian shield-stage lavas, Haleakala

postshield lavas have low SiO_2 contents and high abundances of incompatible elements (2) Haleakala postshield lavas have more depleted isotopic signatures than shield-stage lavas (3) Haleakala postshield lavas, in comparison to shield-stage lavas, are the result of lower melting rates, which are a function of both lower solid mantle upwelling velocities and smaller degrees of melting (see equation 2) (4) Haleakala postshield lavas melted from a source containing residual garnet.

Our dataset provides an opportunity to incorporate constraints on melting processes and sources from major and trace element data, long-lived radiogenic isotope data, and U-series data. While the major and trace elements and long-lived radiogenic isotopes constrain extents of melting and source variability, the U-series data presented here allow us to examine the variation in melting rates across the plume. As we have emphasized above, this melting rate is a function of both F_{max}/d and solid mantle upwelling rates (W). Our modeling shows that the Hana volcanics are the manifestation of both relatively small degrees of melting and lower solid mantle upwelling rates. The solid mantle upwelling rates of Haleakala basanites are at least 10 times lower than shield-stage tholeiites from Kilauea and Mauna Loa. We can therefore use the U-series disequilibria to compare solid mantle upwelling rate to other parameters including the degree of melting and the composition of the source of different Hawaiian lavas. Figure 12 shows comparisons of some relevant geochemical parameters with ($^{230}Th/^{238}U$), ($^{226}Ra/^{230}Th$), and ($^{231}Pa/^{235}U$). SiO_2 is lower in basanites from Haleakala Crater and SWRZ than in other young Hawaiian volcanoes. There is a general negative correlation between SiO_2 and ($^{230}Th/^{238}U$) and ($^{231}Pa/^{235}U$) and also between SiO_2 and ($^{226}Ra/^{230}Th$) if Hualalai data are not considered. The La/Sm ratio is considered a good indicator of the degree of partial melting because of the significantly different partition coefficients of La and Sm ($D_{La}<D_{Sm}$). Haleakala basanites display higher La/Sm than most other young Hawaiian lavas, with the shield-stage lavas of Kilauea and Mauna Loa having the lowest La/Sm ratios within the young Hawaiian lavas examined here. La/Sm ratios correlate well with ($^{230}Th/^{238}U$) and ($^{231}Pa/^{235}U$), suggesting that lower solid mantle upwelling velocities are coupled with smaller degrees of partial melting. We use the

Ba/Ta ratio to investigate the possible presence of a recycled mafic component in the source of Hawaiian lavas. As previously discussed, Haleakala basanites have higher Ba/Ta ratios than most shield-stage Kilauea and Mauna Loa lavas, suggesting that a recycled mafic component is a more likely possibility in the shield-stage lavas than in postshield lavas. Ba/Ta ratios in some Hualalai lavas are as high as or higher than Haleakala basanites, so the Ba/Ta ratio does not distinguish between the sources of Hualalai and Haleakala lavas. In general, lower solid mantle upwelling rates correspond to higher Ba/Ta ratios, and therefore to a more peridotitic source. Last, ε_{Nd} is positively correlated with U-series disequilibria ratios, indicating that more depleted sources are coupled with lower solid mantle upwelling rates.

The postshield Hana Volcanics represent the waning stages of melting of the Hawaiian plume as the Pacific lithosphere moves to the northwest. They are the manifestation of low melting rates (smaller degrees of melting and lower upwelling rates) of a silica-undersaturated depleted source within the plume. As the distance from the plume center increases, rates of solid mantle upwelling decrease by at least a factor of 10. Finally, if a mafic component is present within the Hawaiian plume, it likely was exhausted during shield-stage volcanism before postshield volcanism commenced at Haleakala.

7. CONCLUSIONS

- Haleakala Crater basanites present an opportunity to study the periphery of the Hawaiian plume and to better understand dynamics of mantle upwelling. Geochemical and isotopic analyses of thirteen new samples from Haleakala Crater with ages of less than ~4100 yr B.P. confirm that these late-stage lavas have high alkali contents and enriched incompatible element concentrations, confirming that they are the result of small degrees of partial melting compared to shield-stage tholeiites.
- Haleakala Crater basanites have higher ε_{Nd} and ε_{Hf} and lower $^{87}Sr/^{86}Sr$ isotopic values than shield-stage Hawaiian tholeiites, implying a greater contribution from a

717 depleted source on the periphery of the plume. The Pb isotopes show that the
718 depleted component is unlike Pacific MORB and likely is an intrinsic component to
719 the Hawaiian plume.
720 • The high Ba/Ta ratios, coupled with the depleted isotopic signature, of the Hana
721 Volcanics imply that pyroxenitic or eclogitic lithologies are unlikely in their source.
722 If a mafic component is present within the Hawaiian plume, it is likely exhausted
723 during shield-stage melting, leaving only a depleted peridotitic component to melt
724 during postshield volcanism.
725 • Average ($^{230}Th/^{238}U$), ($^{226}Ra/^{230}Th$), and ($^{231}Pa/^{235}U$) for basanites from
726 Haleakala are all measurably higher than shield-stage tholeiites from Kilauea and
727 Mauna Loa. Dynamic melting models show that the Haleakala basanites result from
728 lower melting rates (which are directly proportional to both the solid mantle
729 upwelling rate and the degree of melting) than the tholeiites. Chromatographic
730 porous flow modeling also confirms that solid mantle upwelling rates and porosity
731 of the melting zone are lower on the periphery of the Hawaiian plume than at the
732 plume center. Specifically, Haleakala Crater basanites have solid mantle upwelling
733 velocities of 0.7-1.0 cm/yr, whereas shield-stage tholeiites have solid mantle
734 upwelling velocities of 10-20 cm/yr.

735 **ACKNOWLEDGEMENTS**
736

737 Funding for this project was provided by NSF grants EAR-0001924 and EAR-
738 9909473 to KWWS. The University of Wyoming Department of Geology and
739 Geophysics, the Wyoming NASA Space Grant Consortium, and the Uranium-series
740 Symposium 2014 provided travel funds to EHP to present results of this research.
741 Matthew Jull is thanked for assistance with fieldwork and Glenn Gaetani is
742 acknowledged for providing thoughtful insights. We thank Terry Plank and
743 colleagues at Boston University for analyzing the major and trace element
744 concentrations. Associate Editor Fred Frey, Andreas Stracke, Aaron Pietruszka, and
745 an anonymous reviewer provided constructive reviews that significantly improved
746 the manuscript. Marc Norman and Shichun Huang are also thanked for editorial
747 handling.

REFERENCES

Abouchami W., Galer S. J. G., and Koschinsky A. (1999) Pb and Nd isotopes in NE Atlantic Fe-Mn crusts: proxies for trace metal paleosources and paleocean circulation. *Geochim. Cosmochim. Acta* **63**, 1489-1505.

Abouchami W., Hofmann A. W., Galer S. J. G., Frey F. A., Eisele J., and Feigenson M. (2005) Lead isotopes reveal bilateral asymmetry and vertical continuity in the Hawaiian mantle plume. *Nature* **434**, 851-856.

Adam J. and Green T. (2006) Trace element partitioning between mica- and amphibole-bearing garnet lherzolite and hydrous basanitic melt: 1. Experimental results and the investigation of controls on partitioning behaviour. *Contrib. Mineral. Petrol.* **152**, 1-17.

Allègre C. J. and Turcotte, D. L. (1986) Implications of a two-component marble-cake mantle. *Nature* **323**, 123–127.

Andersen M. B., Elliott T., Freymuth H., Sims K. W. W., Niu Y., and Kelley K. A. (2015) The terrestrial uranium isotope cycle. *Nature* **517**, 356-359.

Ball, L., Sims K. W. W., and Schwieters J. (2008) Measurement of $^{234}U/^{238}U$ and $^{230}Th/^{232}Th$ in volcanic rocks using the Neptune MC-ICP-MS. *J. Anal. Atom. Spectrom.* **23**, 173-180. doi: 10.1039/b703193a.

Beattie P. (1993) Uranium-thorium disequilibria and partitioning on melting of garnet peridotite. *Nature* **363**, 63-65.

Bergmanis E. C., Sinton J. M. and Trusdell F. A. (2000) Rejuvenated volcanism along the southwest rift zone, East Maui, Hawai'i. *Bull. Volcanol* **62**, 239–255.

Bianco T. A., Ito G., Becker J. M. and Garcia M.O. (2005) Secondary Hawaiian volcanism formed by flexural arch decompression. *Geochem. Geophys. Geosyst.* **6**.

Bizimis M., Salters V. J. M., Garcia, M. O. and Norman M. D. (2013) The composition and distribution of the rejuvenated component across the Hawaiian plume: Hf-Nd-Sr-Pb isotope systematics of Kaula lavas and pyroxenite xenoliths. *Geochem. Geophys. Geosyst.* **14**.

Blichert-Toft J., Frey F. A. and Albarède F. (1999) Hf Isotope Evidence for Pelagic Sediments in the Source of Hawaiian Basalts. *Science* **285**, 879–882.

Bourdon B., Joron J.-L., Claude-Ivanaj C. and Allegre C. J. (1998) U-Th-Pa-Ra systematics for the Grande Comore volcanics: melting processes in an upwelling plume. *Earth Planet. Sci. Lett.* **164**, 119-133.

Bourdon B., Ribe N. M., Stracke A., Saal A. E. and Turner S. P. (2006) Insights into the dynamics of mantle plumes from uranium-series geochemistry. *Nature* **444**, 713–717.

Bourdon B. and Sims K. W. W. (2003). U-series constraints on intraplate magmatism. In: *Uranium Series Geochemistry*, *Reviews in Mineralogy and Geochemistry* **52** (eds. B. Bourdon, G. M. Henderson, C. C. Lundstrom, and S. P. Turner), 215-253. doi: 10.2113/0520215.

Bryce J. G., DePaolo D. J., and Lassiter J. C., (2005) Geochemical structure of the Hawaiian plume: Sr, Nd, and Os isotopes in the 2.8 km HSDP-2 section of Mauna Kea volcano. *Geochem. Geophys. Geosyst.* **6.**

Chabaux F. and Allègre C. J. (1994) ^{238}U-^{230}Th-^{226}Ra disequilibria in volcanics: A new insight into melting conditions. *Earth Planet. Sci. Lett.* **126**, 61–74.

Cheng H., Edwards, R. L., Hoff J., Gallup C. D., Richards D. A., and Asmerom Y. (2000) The half-lives of uranium-234 and thorium-230. *Chem. Geol.*, **169**, 17-33.

Chen, C.-Y. and Frey F. A. (1983) Origin of Hawaiian tholeiite and alkalic basalt. *Nature* **302**, 785–789.

Chen C.-Y. and Frey F. A. (1985) Trace element and isotopic geochemistry of lavas from Haleakala Volcano, East Maui, Hawaii: Implications for the origin of Hawaiian basalts. *J. Geophys. Res.* **90**, 8743–8768.

Chen C.-Y., Frey F. A. and Garcia M. O. (1990) Evolution of alkalic lavas at Haleakala Volcano, east Maui, Hawaii. *Contrib. Mineral. Petrol.* **105**, 197–218.

Chen C.-Y., Frey F. A., Garcia M. O., Dalrymple G. B. and Hart S. R. (1991) The tholeiite to alkalic basalt transition at Haleakala Volcano, Maui, Hawaii. *Contrib. Mineral. Petrol.* **106**, 183–200.

Choi M.S., Francois R., Sims K. W. W., Bacon M. P., Leger-Brown S., Fleer A. P., Ball L., Schneider D., and Pichat S. (2001) Rapid determination of ^{230}Th and ^{231}Pa in seawater by desolvated micro-nebulization Inductively Coupled Plasma magnetic sector mass spectrometry. *Mar. Chem.* **76**, 99-112.

Clague D. A. (1987) Hawaiian alkaline volcanism. In: *Alkaline Igneous Rocks, Geological Society Special Publication No. 30* (ed. J. G. Fitton and B. G. J. Upton). Blackwell Scientific Publications, Oxford.

Clague D. A. and Dalrymple G. B. (1987) The Hawaiian-Emperor volcanic chain Part 1. Geologic evolution. *USGS Prof. Pap.* **1350**, 5-54.

Clague D. A. and Sherrod D. R. (2014) Growth and Degradation of Hawaiian Volcanoes. In: *Characteristics of Hawaiian Volcanoes* (eds. M. P. Poland, T. J. Takahashi, and C. M. Landowski). *U.S. Geological Survey Professional Paper* **1801**, 97-146.

Coe R. S., Singer B. S., Pringle M. S. and Zhao X. (2004) Matuyama-Brunhes reversal and Kamikatsura event on Maui: paleomagnetic directions, ^{40}Ar/^{39}Ar ages and implications. *Earth Planet. Sci. Lett.* **222**, 667-684.

Cohen A. S. and O'Nions R. K., 1993. Melting rates beneath Hawaii: Evidence from uranium series isotopes in recent lavas. *Earth Planet. Sci. Lett.* **120**, 169–175.

Cohen A. S., O'Nions R. K. and Kurz M. D. (1996) Chemical and isotopic variations in Mauna Loa tholeiites. *Earth Planet. Sci. Lett.* **143**, 111–124.

Cooper K. M., Reid M. R., Murrell M. T., and Clague D. A. (2001) Crystal and magma residence at Kilauea Volcano, Hawaii: ^{230}Th-^{226}Ra dating of the 1955 east rift eruption. *Earth Planet. Sci. Lett.* **184**, 703-718.

Cousens B. L. and Clague D. A. (2015) Shield to Rejuvenated Stage Volcanism on Kauai and Niihau, Hawaiian Islands. *J. Petrol.* **56**, 1547-1584.

DePaolo D. J. (1988) *Neodymium Isotope Geochemistry*. Springer-Verlag.

DePaolo D. J. and Stolper E. M. (1996) Models of Hawaiian volcano growth and plume structure: Implications of results from the Hawaii Scientific Drilling Project. *J. Geophys. Res.* **101**, 11643–11654.

Dixon J., Clague D. A., Cousens B., Monsalve M. L., and Uhl J. (2008) Carbonatite and silicate melt metasomatism of the mantle surrounding the Hawaiian plume: Evidence from volatiles, trace elements, and radiogenic isotopes in rejuvenated-stage lavas from Niihau, Hawaii. *Geochem. Geophys. Geosyst.* **9.**

Donnelly K. E., Goldstein S. L., Langmuir C. H., and Spiegelman M. (2004) Origin of enriched ocean ridge basalts and implications for mantle dynamics. *Earth Planet. Sci. Lett.* **226**, 347-366.

Dulaiova H., Sims K. W. W., Charette M. A., Prytulak J., and Blusztajn J. S. (2013) A new method for the determination of low-level actinium-227 in geological samples. *J. RadioAnalytical and Nuclear Chem.* **296**, 279-283.

Elliott T. (1997) Fractionation of U and Th during mantle melting: a reprise. *Chem. Geol.* **139**, 165-183.

Elkins L. J., Gaetani G. A. and Sims K. W. W. (2008) Partitioning of U and Th during garnet pyroxenite partial melting: Constraints on the source of alkaline ocean island basalts. *Earth Planet. Sci. Lett.* **265**, 270–286.

Elkins L. J., Sims K. W. W., Prytulak J., Blichert-Toft J., Elliott T., Blusztajn J., Fretzdorff S., Reagan M., Haase K., Humphris S., and Schilling J.-G. (2014) Melt generation beneath Arctic Ridges: Implications from U decay series disequilibria in the Mohns, Knipovich, and Gakkel Ridges. *Geochim. Cosmochim. Acta* **127**, 140-170.

Elkins L. J., Sims K. W. W., Prytulak J., Elliott T., Mattielli N., Blichert-Toft J., Blusztajn J., Dunbar, N., Devey C., Mertz D. F., Schilling J.-G., Murrell M. (2011) Understanding melt generation beneath the slow-spreading Kolbeinsey Ridge using ^{238}U, ^{230}Th, and ^{231}Pa excesses. *Geochim. Cosmochim. Acta* **75**, 6300-6329.

England J. G., Zindler A., Reisberg L. C., Rubenstone J. L., Salters V., Marcantonio F., Bourdon B., Brueckner H., Turner P. J., Weaver S., and Read P. (1992) The Lamont-Doherty Geological Observatory Isolab 54 isotope ratio mass spectrometer. *Int. J. Mass Spec. Ion Proc.* **121**, 201-240.

Fekiacova Z., Abouchami W., Galer S. J. G., Garcia M. O., and Hofmann A. W. (2007) Origin and temporal evolution of Ko'olau Volcano, Hawai'i: Inferences from isotope data on the Ko'olau

Scientific Drilling Project (KSDP), the Honolulu Volcanics and ODP Site 843. *Earth Planet. Sci. Lett.* **261**, 65-83.

Frey F. A., Huang S., Blichert-Toft J., Regelous M. and Boyet M. (2005) Origin of depleted components in basalt related to the Hawaiian hot spot: Evidence from isotopic and incompatible element ratios. *Geochem. Geophys. Geosyst.* **6**.

Gaffney A. M., Nelson B. K., and Blichert-Toft J. (2004) Geochemical Constraints on the Role of Oceanic Lithosphere in Intra-Volcano Heterogeneity at West Maui, Hawaii. *J. Petrol.* **45**, 1663-1687.

Garcia M. O., Jorgenson B. A., Mahoney J. J., Ito E., and Irving A. J. (1993) An Evaluation of Temporal Geochemical Evolution of Loihi Summit Lavas: Results from *Alvin* Submersible Dives. *J. Geophys. Res.* **98**, 537-550.

Garcia M. O., Pietruszka A. J. and Rhodes J. M. (2003) A Petrologic Perspective of Kilauea Volcano's Summit Magma Reservoir. *J. Petrol* **44**, 2313-2339.

Garcia M. O., Pietruszka A. J., Rhodes J. M., and Swanson K. (2000) Magmatic Processes During the Prolonged Pu'u O'o Eruption of Kilauea Volcano, Hawaii. *J. Petrol.* **41**, 967-990.

Garcia M. O., Rhodes J. M., Trusdell F. A., and Pietruszka A. J. (1996) Petrology of lavas from the Puu Oo eruption of Kilauea Volcano: III. The Kupaianaha episode (1986-1992). *Bull. Volcanol* **58**, 359-379.

Garcia M. O., Rubin K. H., Norman M. D., Rhodes J. M., Graham D. W., Muenow D. W., and Spencer K. (1998) Petrology and geochronology of basalt breccia from the 1996 earthquake swarm of Loihi seamount, Hawaii: magmatic history of its 1996 eruption. *Bull. Volcanol* **59**, 577-592.

Garcia M. O., Swinnard L., Weis D., Greene A. R., Tagami T., Sano H., and Gandy C. E. (2010) Petrology, Geochemistry and Geochronology of Kaua'i lavas over 4.5 Myr: Implications for the Origin of Rejuvenated Volcanism and the Evolution of the Hawaiian Plume. *J. Petrol.* **51**, 1507-1540.

Hart S. R., Ball L., and Jackson M. (2005) Sr isotopes by laser ablation PIMMS: application to CPX from Samoan peridotite xenoliths. WHOI Plasma Facility Open File Technical Report, vol. 11. www.whoi.edu/science/GG/people/shart/open_file.htm

Hart S. R. and Blusztajn J. (2006) Age and geochemistry of the mafic sills, ODP site 1276, New Foundland margin. *Chem. Geol.* **235**, 222-237. doi: 10.1016/j.chemgeo.2006.07.001.

Hart S. R., Hauri E. H., Oschmann L. A. and Whitehead J. A. (1992) Mantle Plumes and Entrainment: Isotopic Evidence. *Science* **256**, 517-520.

Hart S. R., Workman R. K., Ball L., and Blusztajn J. (2004) High precision Pb isotope techniques from the WHOI NEPTUNE PIMMS. WHOI Plasma Facility Open File Technical Report, vol. 10. www.whoi.edu/science/GG/people/shart/open_file.htm

Hauri E. H. (1996) Major-element variability in the Hawaiian mantle plume. *Nature* **382**, 415–419.

Hauri E. H., Whitehead J. A. and Hart S. R. (1994) Fluid dynamic and geochemical aspects of entrainment in mantle plumes. *J. Geophys. Res.* **99**, 24275–24300.

Hirschmann M. M., Kogiso T., Baker M. B. and Stolper E. M. (2003) Alkalic magmas generated by partial melting of garnet pyroxenite. *Geology* **31**, 481-484.

Hirschmann M. M. and Stolper E. M. (1996) A possible role for garnet pyroxenite in the origin of the "garnet signature" in MORB. *Contrib. Mineral. Petrol.* **124**, 185-208.

Hofmann A. W. and Farnetani C.G. (2013) Two views of Hawaiian plume structure. *Geochem. Geophys. Geosyst.* **14.**

Holden N. E. (1990) Total half-lives for selected nuclides. *Pure Appl. Chem.* **62**, 941-958.

Huang S., Frey F. A., Blichert-Toft J., Fodor R. V., Bauer G. R. and Xu G. (2005) Enriched components in the Hawaiian plume: Evidence from Kahoolawe Volcano, Hawaii. *Geochem. Geophys. Geosyst.* **6**.

Ito G. and Mahoney J. J. (2005) Flow and melting of a heterogeneous mantle: 1. Method and importance to the geochemistry of ocean island and mid-ocean ridge basalts. *Earth Planet. Sci. Lett.* **230**, 29-46.

Jackson M. G., Weis D. and Huang S. (2012) Major element variations in Hawaiian shield lavas: Source features and perspectives from global ocean island basalt (OIB) systematics. *Geochem. Geophys. Geosyst.* **13**.

Jaffey A. H., Flynn K. F., Glendenin L. E., Bentley W. C., and Essling A. M. (1971) Precision measurement of half-lives and specific activities of ^{235}U and ^{238}U, *Phys. Rev. C*, **4**, 1889-1906.

Kay R. W. (1980) Volcanic Arc Magmas: Implications of a melting-mixing model for element recycling in the crust-upper mantle system. *J. Geol.* **88**, 497-522.

Kelley K. A., Plank T., Ludden J., and Staudigel H. (2003) Composition of altered oceanic crust at ODP sites 801 and 1149. *Geochem. Geophys. Geosyst.* **4**, doi: 10.1029/2002GC000435.

Klein E. M. and Langmuir C. H. (1987) Global Correlations of Ocean Ridge Basalt Chemistry with Axial Depth and Crustal Thickness. *J. Geophys. Res.* **92**, 8089-8115.

Kogiso T., Hirschmann M. M. and Frost D. J. (2003) High-pressure partial melting of garnet pyroxenite: possible mafic lithologies in the source of ocean island basalts. *Earth Planet. Sci. Lett.* **216**, 603-617.

Lassiter J. C., DePaolo D. J. and Tatsumoto M. (1996) Isotopic evolution of Mauna Kea volcano: Results from the initial phase of the Hawaii Scientific Drilling Project. *J. Geophys. Res.* **101**, 11769–11780.

Lassiter J. C., Hauri E. H., Reiners P. W. and Garcia M. O. (2000) Generation of Hawaiian post-erosional lavas by melting of a mixed lherzolite/pyroxenite source. *Earth Planet. Sci. Lett.* **178**, 269-284.

LaTourrette T. Z., Kennedy A. K. and Wasserburg G. J. (1993) U-Th fractionation by garnet-evidence for a deep source and rapid rise by oceanic basalts. *Science* **261**, 739-742.

Le Roux L. J. and Glendenin L. E. (1963) Half-life of ^{232}Th, *Proc. Natl. Meet. Nucl. Energy*, **83**.

Lundstrom C. C., Hoernle K. and Gill J. (2003) U-series disequilibria in volcanic rocks from the Canary Islands: Plume versus lithospheric melting. *Geochim. Cosmochim. Acta* **67**, 4153-4177.

Lundstrom C. C., Shaw H. F., Ryerson F. J., Phinney D. L., Gill J. B. and Williams, Q. (1994) Compositional controls on the partitioning of U, Th, Ba, Pb, Sr and Zr between clinopyroxene and haplobasaltic melts: implications for uranium series disequilibria in basalts. *Earth Planet. Sci. Lett.* **128**, 407–423.

Macdonald G. A. and Abbott A. T. (1970) Volcanoes in the sea; the geology of Hawaii. University of Hawaii Press, Honolulu.

Macdonald G. A. and Powers H. A. (1968) A Further Contribution to the Petrology of Haleakala Volcano, Hawaii. *Geol. Soc. Am. Bull.* **79**, 877–888.

Marske J. P., Garcia M. O., Pietruszka A. J., Rhodes J. M., and Norman M. D. (2008) Geochemical Variations during Kīlauea's Pu'u 'Ō'ō Eruption Reveal a Fine-scale Mixture of Mantle Heterogeneities within the Hawaiian Plume. *J. Petrol.* **49**, 1297-1318.

Matzen A. K., Baker M. B., Beckett J. R., and Stolper E. M. (2013) The Temperature and Pressure Dependence of Nickel Partitioning between Olivine and Silicate Melt. *J. Petrol.* **54**, 2521-2545.

McDonough W. F. and Sun S.-s. (1995) The composition of the Earth. *Chem. Geol.* **120**, 223-253.

McKay G. A. (1989) Partitioning of REE between major silicate minerals and basaltic melts. In: *Geochemistry and Mineralogy of REE* (eds. B. R. Lipin and G. A. McKay). *Reviews in Mineralogy* **21**, 45-75.

McKenzie D. (1985) ^{230}Th^{238}U disequilibrium and the melting processes beneath ridge axes. *Earth Planet. Sci. Lett.* **72**, 149–157.

Morgan W. J. (1971) Convection Plumes in the Lower Mantle. *Nature* **230**, 42–43.

Munker C., Weyer, S., Scherer E., and Mezger, K. (2001) Separation of high field strength elements (Nb, Ta, Zr, Hf) and Lu from rock samples for MC-ICPMS measurements. *Geochem. Geophys. Geosyst.* **2**.

Nielsen S. G., Rehkämper M., Norman M. D., Halliday A. N., and Harrison D. (2006) Thallium isotopic evidence for ferromanganese sediments in the mantle source of Hawaiian basalts. *Nature* **439**, 314-317.

Nobra Silva I. G., Weis D., and Scoates J. S. (2013) Isotopic systematics of the early Mauna Kea shield phase and insight into the deep mantle beneath the Pacific Ocean. *Geochem. Geophys. Geosyst.* **14**.

Oostdam B. L. (1965) Age of lava flows on Haleakala, Maui, Hawaii. *Geol. Soc. Am. Bull.* **76**, 393-394.

Pearce J. A. and Stern R. J. (2006) Origin of Back-Arc Basin Magmas: Trace Element and Isotope Perspectives. In: *Back-Arc Spreading Systems: Geological, Biological, Chemical, and Physical Interactions; Geophysical Monograph 166*, 63-86.

Pertermann M. and Hirschmann M. M. (1999) Partial melting experiments on a MORB-like pyroxenite between 2 and 3 GPa: Constraints on the presence of pyroxenite in basalt source regions from solidus location and melting rate. *J. Geophys. Res.* **108**.

Pertermann M. and Hirschmann M.M. (2002) Trace-element partitioning between vacancy-rich eclogitic clinopyroxene and silicate melt. *Am Mineral* **87**, 1365-1376.

966 Pertermann M., Hirschmann M.M., Hametner K., Günther D., and Schmidt M.W. (2004) Experimental
967 determination of trace element partitioning between garnet and silica-rich liquid during
968 anhydrous partial melting of MORB-like eclogite. *Geochem. Geophys. Geosyst.* **5,**
969 doi:10.1029/2003GC000638.
970 Pichat S., Sims K. W. W., François R., McManus J. F., Brown Leger S., and Albarède F. (2004) Lower
971 export production during glacial periods in the equatorial Pacific as derived from (^{231}Pa/^{230}Th)
972 measurements in deep-sea sediments. *Paleoceanography* **19**, PA4023, doi:
973 10.1029/2003PA000994.
974 Pickett, D. A. and Murrell M. T. (1997) Observations of ^{231}Pa/^{235}U disequilibrium in volcanic rocks.
975 *Earth Planet. Sci. Lett.* **148**, 259-271.
976 Pietruszka A. J. and Garcia M. O. (1999) The size and shape of Kilauea Volcano's summit magma
977 storage reservoir: a geochemical probe. *Earth Planet. Sci. Lett.* **167**, 311-320.
978 Pietruszka A. J., Hauri E. H., Carlson R. W., and Garcia M. O. (2006) Remelting of recently depleted
979 mantle within the Hawaiian plume inferred from the ^{226}Ra-^{230}Th-^{238}U disequilibria of Pu'u 'Ō'ō
980 eruption lavas. *Earth Planet. Sci. Lett.* **244**, 155-169.
981 Pietruszka A. J., Keyes M. J., Duncan J. A., Hauri E. H., Carlson R. W., and Garcia M. O. (2011) Excesses
982 of seawater-derived ^{234}U in volcanic glasses from Loihi Seamount due to crustal contamination.
983 *Earth Planet. Sci. Lett.* **304,** 280-289.
984 Pietruszka A. J., Norman M. D., Garcia M. O., Marske J. P., and Burns D. H. (2013) Chemical
985 heterogeneity in the Hawaiian mantle plume from the alteration and dehydration of recycled
986 oceanic crust. *Earth Planet. Sci. Lett.* **361**, 298-309.
987 Pietruszka A. J., Rubin K. H. and Garcia M. O. (2001) ^{226}Ra–^{230}Th–^{238}U disequilibria of historical
988 Kilauea lavas (1790–1982) and the dynamics of mantle melting within the Hawaiian plume.
989 *Earth Planet. Sci. Lett.* **186**, 15–31.
990 Prytulak J. and Elliott T. (2009) Determining melt productivity of mantle sources from ^{238}U-^{230}Th and
991 ^{235}U-^{231}Pa disequilibria; an example from Pico Island, Azores. *Geochim. Cosmochim. Acta* **73**,
992 2103-2122.
993 Putirka K. (2008) Excess temperatures at ocean islands: Implications for mantle layering and
994 convection. *Geology* **36**, 283-286.
995 Ren Z.-Y., Hanyu T., Miyazaki T., Chang Q., Kawabata H., Takahashi T., Hirahara Y., Nichols A. R. L. and
996 Tatsumi Y. (2009) Geochemical Differences of the Hawaiian Shield Lavas: Implications for
997 Melting Process in the Heterogeneous Hawaiian Plume. *J. Petrol.* **50**, 1553–1573.
998 Ren Z.-Y., Shibata T., Yoshikawa M., Johnson K. T. M., and Takahashi E. (2006) Isotope compositions of
999 the submarine Hana Ridge lavas, Haleakala volcano, Hawaii: Implications for source
1000 compositions, melting process and the structure of the Hawaiian plume. *J. Petrol.* **47**, 255-275.
1001 Ribe N. M. and Christensen U.R. (1994) Three-dimensional modeling of plume-lithosphere
1002 interaction. *J. Geophys. Res.* **99**, 669–682.
1003 Ribe N. M. and Christensen U. R. (1999) The dynamical origin of Hawaiian volcanism. *Earth Planet.*
1004 *Sci. Lett.* **171**, 517–531.
1005 Robert J., Miranda C. F., and Muxart R. (1969) Mesure de la periode du protactinium-231 par
1006 microcalorimetrie, *Radiochim. Acta*, **11**, 104-108.
1007 Rubin K. H., van der Zander I., Smith M. C., and Bergmanis E. C. (2005) Minimum speed limit for ocean
1008 ridge magmatism from ^{210}Pb-^{226}Ra-^{230}Th disequilibria. *Nature* **437**, 534-538.
1009 Rudge J. F., Maclennan J., and Stracke A. (2013) The geochemical consequences of mixing melts from
1010 a heterogeneous mantle. *Geochim. Cosmochim. Acta* **114**, 112-143.
1011 Salters, V. J. M., Blichert-Toft J., Fekiacova Z., Sachi-Kocher A., and Bizimis M. (2006) Isotope and trace
1012 element evidence for depleted lithosphere in the source of enriched Ko'olau basalts. *Contrib.*
1013 *Mineral. Petrol.* **151**, 297-312.
1014 Salters V. J. M. and Hart S. R. (1989) The Hf-paradox, and the role of garnet in the MORB source.
1015 *Nature* **342**, 420-422.
1016 Salters V. J. M. and Longhi J. (1999) Trace element partitioning during the initial stages of melting
1017 beneath mid-ocean ridges. *Earth Planet. Sci. Lett.* **166**, 15–30.
1018 Salters V. J. M., Longhi J. E. and Bizimis M. (2002) Near mantle solidus trace element partitioning at
1019 pressures up to 3.4 GPa. *Geochem. Geophys. Geosyst.* **3**.

Salters V. J. M. and Sachi-Kocher A. (2010) An ancient metasomatic source for the Walvis Ridge basalts. *Chem. Geol.* **273**, 151-167.

Salters V. J. M. and Stracke A. (2004) Composition of the depleted mantle. *Geochem. Geophys. Geosyst.* **5**.

Salters V. J. M. and White W. M. (1998) Hf isotope constraints on mantle evolution. *Chem. Geol.* **145**, 447-460.

Sherrod D. R., Hagstrum J. T., McGeehin J. P., Champion D. E. and Trusdell F. A. (2006) Distribution, ^{14}C chronology, and paleomagnetism of latest Pleistocene and Holocene lava flows at Haleakalā volcano, Island of Maui, Hawai'i: A revision of lava flow hazard zones. *J. Geophys. Res.* **111**.

Sherrod D. R. and McGeehin J. P. (1999) New Radiocarbon ages from Haleakala Crater, Island of Maui, Hawaii. USGS Open-File Report 99-143.

Sherrod D. R., Nishimitsu Y. and Tagami T. (2003) New K-Ar ages and the geologic evidence against rejuvenated-stage volcanism at Haleakalā, East Maui, a postshield-stage volcano of the Hawaiian island chain. *Geol. Soc. Am. Bull.* **115**, 683–694.

Sims K. W. W., Blichert-Toft J., Kyle P. R., Pichat S., Gauthier P., Blusztajn J., Kelly P., Ball L. and Layne G. (2008a) A Sr, Nd, Hf, and Pb isotope perspective on the genesis and long-term evolution of alkaline magmas from Erebus volcano, Antarctica. *J. Volcanol. Geoth. Res.* **177**, 606-618.

Sims K. W. W., DePaolo D. J., Murrell M. T., Baldridge W. S., Goldstein S. J. and Clague D. A. (1995) Mechanisms of Magma Generation Beneath Hawaii and Mid-Ocean Ridges: Uranium/Thorium and Samarium/Neodymium Isotopic Evidence. *Science* **267**, 508–512.

Sims K. W. W., DePaolo D. J., Murrell M. T., Baldridge W. S., Goldstein S., Clague D. and Jull M. (1999) Porosity of the melting zone and variations in the solid mantle upwelling rate beneath Hawaii: inferences from ^{238}U-^{230}Th-^{226}Ra and ^{235}U-^{231}Pa disequilibria. *Geochim. Cosmochim. Acta* **63**, 4119–4138, doi: 10.1016/S0016-7037(99)00313-0.

Sims K. W. W., Gill J. B., Dossetto A., Hoffmann D. L., Lundstrom C. C., Williams R. W., Ball L., Tollstrup D., Turner S., Prytulak J., Glessner J. J. G., Standish J. J., and Elliott T. (2008b) An inter-laboratory assessment of the Th Isotopic Composition of Synthetic and Rock standards. *Geostand. Geoanal. Res.* **32**, 65-91. doi: 10.1111/j.1751-908X.2008.00870.x.

Sims K. W. W., Goldstein S. J., Blichert-Toft J., Perfit M. R., Kelemen P., Fornari D. J., Michael P., Murrell M. T., Hart S. R., DePaolo D. J., Layne G., Ball L., Jull M., and Bender P. (2002) Chemical and isotopic constraints on the generation and transport of magma beneath the East Pacific Rise. *Geochim. Cosmochim. Acta* **66**, 3481-3504.

Sims K. W. W. and Hart S. R. (2006) Comparison of Th, Sr, Nd and Pb isotopes in oceanic basalts: Implications for mantle heterogeneity and magma genesis. *Earth Planet. Sci. Lett.* **245**, 743-761.

Sims K. W. W., Hart S. R., Reagan M. K., Blusztajn J., Staudigel H., Sohn R. A., Layne G. D., Ball L. A., and Andrews J. (2008c) ^{238}U-^{230}Th-^{226}Ra-^{210}Pb-^{210}Po, ^{232}Th-^{228}Ra and ^{235}U-^{231}Pa constraints on the ages and petrogenesis of Vailulu and Malumalu Lavas, Samoa. *Geochem. Geophys. Geosyst.* **9.**

Sims, K. W. W., Maclennan J., Blichert-Toft J., Mervine, E. M., Blusztajn J., and Grönvold K. (2013) Short length scale mantle heterogeneity beneath Iceland probed by glacial modulation of melting. *Earth Planet. Sci. Lett.* **379**, 146-157.

Sleep N. H. (1990) Hotspots and Mantle Plumes: Some Phenomenology. *J. Geophys. Res.* **95**, 6715–6736.

Sobolev A. V., Hofmann A. W., Sobolev S. V. and Nikogosian I. K. (2005) An olivine-free mantle source of Hawaiian shield basalts. *Nature* **434**, 590–597.

Spiegelman M. (2000) UserCalc: a web-based Uranium series calculator for magma-migration problems.

Spiegelman M. and Elliott T. (1993) Consequences of melt transport for uranium series disequilibrium in young lavas. *Earth Planet. Sci. Lett.* **118**, 1–20.

Stearns H. T. (1940) Four-phase volcanism in Hawaii. *Geol. Soc. Am. Bull.* **51**, 1947–1948.

Stearns H. T. and Macdonald G. A. (1942) Geology and ground-water resources of the island of Maui, Hawaii (including Haleakala section, Hawaii National Park). Advertiser Pub. Co., Honolulu.

Stracke A. and Bourdon B. (2009) The importance of melt extraction for tracing mantle heterogeneity. *Geochim. Cosmochim. Acta* **73**, 218-238.

Stracke A., Bourdon B., and McKenzie D. (2006) Melt extraction in the Earth's mantle: Constraints from U-Th-Pa-Ra studies in oceanic basalts. *Earth Planet. Sci. Lett.* **244**, 97-112.

Stracke A., Salters V. J. M. and Sims K. W. W. (1999) Assessing the presence of garnet-pyroxenite in the mantle sources of basalts through combined hafnium-neodymium-thorium isotope systematics. *Geochem. Geophys. Geosyst.* **1**, 1–13.

Tanaka R., Makishima A., and Nakamura E. (2008) Hawaiian double volcanic chain triggered by an episodic involvement of recycled material: Constraints from temporal Sr-Nd-Hf-Pb isotopic trend of the Loa-type volcanoes. *Earth Planet. Sci. Lett.* **265**, 450-465.

Tanaka R., Nakamura E., and Takahashi E. (2002) Geochemical Evolution of Koolau Volcano, Hawaii. In: *Hawaiian Volcanoes: Deep Underwater Perspectives; Geophysical Monograph 128*, 311-332.

Taras B. D. and Hart S. R. (1987) Geochemical evolution of the New England seamount chain: Isotopic and trace-element constraints. *Chem. Geol.* **64**, 35-54.

Todt W., Cliff R. A., Hanser A., and Hofmann A.W. (1996) Evaluation of a ^{202}Pb-^{205}Pb double spike for high-precision lead isotope analysis. In: Earth processes, reading the isotopic code, **95** (eds. S. R. Hart and A. Basu) AGU, 429-437.

Tuli D. (2000) Nuclear wallet cards, 114 p. Brookhaven Natl. Lab., Upton, N.Y.

van Westrenen W., Blundy J., and Wood B. (1999) Crystal-chemical controls on trace element partitioning between garnet and anhydrous silicate melt. *Am. Min.* **84**, 838-847.

Wagner T. P. and Grove T. L. (1998) Melt/harzburgite reaction in the petrogenesis of tholeiitic magma from Kilauea volcano, Hawaii. *Contrib. Mineral. Petrol.* **131**, 1-12.

Wang Z. and Gaetani G. A. (2008) Partitioning of Ni between olivine and siliceous eclogite partial melt: experimental constraints on the mantle source of Hawaiian basalts. *Contrib. Mineral. Petrol.* **156**, 661-678.

Waters C. L., Sims K. W. W., Perfit M. R., Blichert-Toft J., and Blusztajn J. (2011) Perspective on the Genesis of E-MORB from Chemical and Isotopic Heterogeneity at 9-10°N East Pacific Rise. *J. Petrol.* **52**, 565-602.

Watson S. and McKenzie D. (1991) Melt Generation by Plumes - A Study of Hawaiian Volcanism. *J. Petrol.* **32**, 501–537.

Wendt J. I., Regelous M., Niu Y., Hékinian R., and Collerson K. D. (1999) Geochemistry of lavas from the Garrett Transform Fault: insights into mantle heterogeneity beneath the eastern Pacific. *Earth Planet. Sci. Lett.* **173**, 271-284.

Weis D., Garcia M. O., Rhodes J. M., Jellinek M. and Scoates J. S. (2011) Role of the deep mantle in generating the compositional asymmetry of the Hawaiian mantle plume. *Nature Geosci.* **4**, 831–838.

West H. B. and Leeman W. P. (1987) Isotopic evolution of lavas from Haleakala Crater, Hawaii. *Earth Planet. Sci. Lett.* **84**, 211–225.

Weatherly S. M. and Katz R. F. (2016) Melt transport rates in heterogeneous mantle beneath mid-ocean ridges. *Geochim. Cosmochim. Acta* **172**, 39-54.

White, W. M., Albarède F., and Telouk P. (2000) High-precision analysis of Pb isotope ratios by multi-collector ICP-MS. *Chem. Geol.* **167**, 257-270.

Wilson J. T., (1963) A possible origin of the Hawaiian Islands. *Can. J. Phys.* **41**, 863–870.

Wolfe C. J., Solomon S. C., Laske G., Collins J. A., Detrick R. S., Orcutt J. A., Bercovici D. and Hauri E. H. (2011) Mantle P-wave velocity structure beneath the Hawaiian hotspot. *Earth Planet. Sci. Lett.* **303**, 267-280.

Workman R. K., Hart S. R., Jackson M., Regelous M., Farley K. A., Blusztajn J., Kurz M. and Staudigel H. (2004) Recycled metasomatized lithosphere as the origin of the Enriched Mantle II (EM2) end-member: Evidence from the Samoan Volcanic Chain. *Geochem. Geophys. Geosyst.* **5**.

Xu G., Frey F. F., Clague D. A., Weis D., and Beeson M. H. (2005) East Molokai and other Kea-trend volcanoes: Magmatic processes and sources as they migrate away from the Hawaiian hot spot. *Geochem. Geophys. Geosyst.* **6**.

Yogodzinski G. M., Brown S. T., Kelemen P. B., Vervoort J. D., Portnyagin M., Sims K. W. W., Hoernle K., Jicha B. R. and Werner R. (2015) The Role of Subducted Basalt in the Source of Island Arc Magmas: Evidence from Seafloor Lavas of the Western Aleutians. *J. Petrol.* **0**, 1-52.

Zhao D., Yamamoto Y. and Yanada T. (2013) Global mantle heterogeneity and its influence on teleseismic regional tomography. *Gondwana Res.* **23**, 595-616.

Zindler A. and Hart S. R. (1986) Chemical geodynamics. *Annu. Rev. Earth Planet. Sci.* **14**, 493-571.

Figure Captions

Figure 1: Map of Maui (top) highlighting the Hana Volcanics and map of Haleakala Crater (bottom) with locations of the 13 new samples presented in this paper, marked with purple stars. Ages for samples dated by ^{14}C are shown (Sherrod and McGeehin, 1999). Kea and Loa trends on general location map from Weis et al. (2011).

Figure 2: Total alkalis vs. silica diagram comparing Haleakala lavas to averages for other Hawaiian volcanoes. Measured SiO_2 content is plotted and is not corrected for olivine fractionation because samples were picked free of phenocrysts prior to analysis. Haleakala Crater basanites from this study are shown as red diamonds and SWRZ samples (Sims et al., 1999) as red squares. Literature data for the Kula and Hana Volcanics are grouped together and include Hana lavas designated as either postshield or rejuvenated stage in the original work. The GEOROC database was used to compile comparison data for this figure and subsequent figures. Entries in the GEOROC database that come from references older than 1980, are not volcanic rocks, or are denoted as altered were not included in any comparison data. See supplement for full list of references used in comparison data. In Figure 2, averages for various stages of Hawaiian volcanoes include data entries for which an eruptive stage (e.g., postshield) is designated in the GEOROC database. Hualalai averages do not include trachyte lavas. L.D. denotes literature data.

Figure 3: Trace element diagram comparing the Hana Volcanics with averages for other Hawaiian volcanoes and Pacific MORB. Averages for Kilauea, Mauna Loa, Mauna Kea, Hualalai, and Loihi include data from all eruptive stages. Hualalai trachytes are excluded from average. Element concentrations normalized to primitive mantle values of McDonough and Sun (1995). See supplement for full list of references used in comparison data. L.D. denotes literature data.

Figure 4: $^{87}Sr/^{86}Sr$ versus ε_{Nd} showing the depleted isotopic signature of Haleakala Crater, SWRZ and other postshield lavas compared to other Hawaiian volcanoes. Literature data for the Kula and Hana Volcanics are grouped together and include Hana lavas designated as either postshield or rejuvenated stage in the original work; this group is distinguished from literature data for the shield-stage Honomanu Basalt, which is >0.93 Ma. Inset displays the range in Hawaiian data compared to OIB and Pacific MORB. Mantle end member compositions from the following sources: DMM (Salters and Stracke, 2004; extreme D-MORB); HIMU and EM1 (Hart et al., 1992; Zindler and Hart, 1986); EM2 (Workman et al., 2004). See supplement for full list of references used in comparison data. L.D. denotes literature data.

Figure 5: ε_{Nd} versus ε_{Hf} showing the depleted isotopic signature of Haleakala Crater, SWRZ and other postshield lavas compared to other Hawaiian volcanoes. For SWRZ samples, Nd isotopic data reported in Sims et al. (1999) and Hf isotopic data reported in Stracke et al. (1999). Literature data for the Kula and Hana Volcanics are grouped together and include Hana lavas designated as either postshield or rejuvenated stage in the original work; this group is distinguished from literature data for the shield-stage Honomanu Basalt, which is >0.93 Ma. Inset displays the range in Hawaiian data compared to OIB and Pacific MORB. Mantle end member composition for DMM from Salters and Stracke (2004; extreme D-MORB). Neodymium isotopic composition for HIMU and EM1 from Hart et al. (1992) and Zindler and Hart (1986) and EM2 from Workman et al. (2004). Hafnium isotopic composition for HIMU, EM1 and EM2 from Salters and White (1998). See supplement for full list of references used in comparison data. L.D. denotes literature data.

Figure 6: (a.) $^{206}Pb/^{204}Pb$ vs. $^{208}Pb/^{204}Pb$ and (b.) $^{206}Pb/^{204}Pb$ vs. $^{87}Sr/^{86}Sr$ comparing Haleakala Crater, SWRZ, and other postshield lavas to other Hawaiian volcanoes. For SWRZ samples Sr isotopic data reported in Sims et al. (1999) and Pb isotopic data reported in Table 3. Literature data for the Kula and Hana Volcanics are grouped together and include Hana lavas designated as either postshield or

1193 rejuvenated stage in the original work; this group is distinguished from literature
1194 data for the shield-stage Honomanu Basalt, which is >0.93 Ma. Black line in (a.) is
1195 from Abouchami et al. (2005) and Weis et al. (2011) and divides Loa trend
1196 volcanoes (Mauna Loa, Hualalai, and Loihi) from Kea trend volcanoes (Mauna Kea,
1197 Kilauea, and Haleakala). Pink lines in (b.) outline the ranges of Pacific MORB data for
1198 the Garrett Transform from Wendt et al. (1999) and axial East Pacific Rise (EPR)
1199 samples from 9°50'N and 9°30'N from Sims et al. (2002). Lead isotope comparison
1200 data from the literature include measurements made by MC-ICP-MS, double-spike
1201 TIMS, and conventional TIMS. See supplement for full list of references used in
1202 comparison data. L.D. denotes literature data.
1203
1204 Figure 7: Ce/Sm (normalized to primitive mantle values of McDonough and Sun,
1205 1995) vs. $^{87}Sr/^{86}Sr$, ε_{Nd}, and $^{208}Pb/^{206}Pb$. Haleakala Crater data from this study,
1206 Haleakala SWRZ from Sims et al. (1999), and other Haleakala data from the Kula and
1207 Hana Volcanics from multiple literature sources (see supplement). Literature data
1208 for the Kula and Hana Volcanics are grouped together and include Hana lavas
1209 designated as either postshield or rejuvenated stage in the original work. We
1210 assume Kilauea tholeiites most closely represent the most recent eruptive products
1211 from the center of the Hawaiian plume (Bryce et al., 2005; DePaolo and Stolper,
1212 1996). Squares are averages for Haleakala postshield lavas (red), Kilauea (green),
1213 and Pacific MORB (gray). Triangles are calculated initial solid source values. For this
1214 calculation we use a batch melting equation and melt fractions of 3% for Haleakala
1215 postshield lavas, 15% for Kilauea lavas, and 20% for Pacific MORB lavas. These melt
1216 fractions are based on modeled melt fractions for Hawaiian lavas by Sims et al.
1217 (1999) and the maximum amount of mantle melting predicted at ocean ridges by
1218 Klein and Langmuir (1987). Bulk distribution coefficients for garnet peridotite (59%
1219 olivine, 21% opx, 8% cpx, 12% garnet) are 0.0065 for Ce and 0.0474 for Sm. We plot
1220 the Ce/Sm ratios in order to utilize self-consistent partition coefficients from Salters
1221 and Longhi (1999) and Salters et al. (2002), who do not report La partitioning data;
1222 an average of the partition coefficients of all experiments at pressures >2.4 GPa from

both publications were used for cpx, opx, and garnet; the partition coefficient for olivine from the 1 GPa experiment was used because higher pressure experimental data was not given. Utilization of different partition coefficients (e.g., Adam and Green, 2006 for basanites) shifts the initial solid values slightly to the left or right on this plot, but does not affect the interpretation of the model. Also shown are the isotopic values of the Depleted Rejuvenated Component (DRC) of Bizimis et al. (2013) in blue ($^{87}Sr/^{86}Sr$ for the DRC is defined as <0.70305) and the isotopic values of the Depleted Makapuu component (DMK) of Tanaka et al. (2008) in orange. Based on Sr and Nd isotopic data the Haleakala solid mantle source could be a two-component mix of the Pacific MORB and plume (Kilauea) initial solids. The Pb isotope data, however, suggest that this is not the case and that the Haleakala initial solid is likely a mixture of plume material and a high $^{208}Pb/^{206}Pb$ component, possibly an extreme Pacific MORB composition, the DRC of Bizimis et al. (2013), or the DMK component of Tanaka et al. (2008). Lead isotope comparison data from the literature include measurements made by MC-ICP-MS, double-spike TIMS, and conventional TIMS. See supplement for full list of references used in comparison data. L.D. denotes literature data.

Figure 8: ε_{Nd} versus Ba/Ta for Haleakala Crater, SWRZ and other postshield lavas compared to other Hawaiian volcanoes. For SWRZ samples, Nd isotopic data reported in Sims et al. (1999). Literature data for the Kula and Hana Volcanics are grouped together and include Hana lavas designated as either postshield or rejuvenated stage in the original work; this group is distinguished from literature data for the shield-stage Honomanu Basalt, which is >0.93 Ma. See supplement for full list of references used in comparison data. L.D. denotes literature data.

Figure 9: ($^{230}Th/^{238}U$) vs. ($^{231}Pa/^{235}U$) (top) and ($^{230}Th/^{238}U$) vs. ($^{226}Ra/^{230}Th$) (bottom) for Hawaiian lavas. Pickett and Murrell (1997) report ($^{231}Pa/^{235}U$) for select Hawaiian samples for which other U-series data are reported in Sims et al. (1999). ($^{230}Th/^{238}U$) and ($^{226}Ra/^{230}Th$) data for one whole rock sample from Cooper et al. (2001) is included in comparison data. Grid lines represent dynamic melting

models (after McKenzie, 1985) and show that melting rates for Haleakala basanites are between approximately $1x10^{-5}$ and $1x10^{-4}$ kg m^{-3} yr^{-1} with melt-zone porosity from 0.2% to 0.5%, significantly lower than shield-stage tholeiites.

Figure 10: Chromatographic porous flow modeling using the web-based UserCalc program of Spiegelman (2000) for Kilauea and Mauna Loa tholeiites (a), Hualalai alkali basalts (b), and Haleakala basanites (c). This program is based on the chromatographic models of Spiegelman and Elliott (1993). The contour plots model the solid mantle upwelling velocity and porosity of the melt zone using three U-series nuclide pairs (red for ($^{230}Th/^{238}U$); green for ($^{226}Ra/^{230}Th$); blue for ($^{231}Pa/^{235}U$)). The point at which the three lines coincide is the modeled porosity and solid mantle upwelling velocity. Average disequilibria values for tholeiites are shown in the left plot and include data from Cohen and O'Nions (1993), Cohen et al. (1996), Cooper et al. (2001; whole rock data), Pickett and Murrell, (1997), Pietruszka et al. (2001; 2006), and Sims et al. (1999). Average disequilibria values for Hualalai alkali basalts from Pickett and Murrell (1997) and Sims et al. (1999) are shown in the middle plot. Average disequilibria values for Haleakala basanites are shown in the right plot and include new Haleakala Crater lavas and Haleakala SWRZ lavas (Pickett and Murrell, 1997; Sims et al., 1995; 1999). Models were produced using inverted D values for U and Th for garnet peridotite source of Sims et al. (1999) and for Ra and Pa from Lundstrom et al. (1994). Error envelopes (dashed) signify 1 standard deviation of the mean values. The upper error bound for ($^{230}Th/^{238}U$) for the tholeiites is outside the plotted area (a).

Figure 11: Alpha Sm/Nd vs. ($^{230}Th/^{238}U$) for Hawaiian volcanoes. Alpha Sm/Nd represents Sm/Nd fractionation and is defined as $(Sm/Nd)_{magma}/(Sm/Nd)_{source}$. Batch melting and accumulation fractional melting models for a garnet lherzolite source (12% garnet, 8% cpx, 21% opx, 59% olivine) utilize the following D values: $D_{Sm} = 0.04$; $D_{Nd} = 0.02$; $D_{Th} = 0.0026$; $D_U = 0.0052$ (McKay, 1989; Salters and Longhi, 1999; Salters et al., 2002). Alpha Sm/Nd for Kilauea calculated from data in Garcia et al. (1996; 2000) Marske et al. (2008), and Pietruszka et al. (2006). Alpha Sm/Nd for

Loihi calculated from data in Garcia et al. (1993; 1998) and Pietruszka et al. (2011; corrected ($^{230}Th/^{238}U$) values).

Figure 12: ($^{230}Th/^{238}U$), ($^{226}Ra/^{230}Th$), and ($^{231}Pa/^{235}U$) versus SiO_2, La/Sm, Ba/Ta, and ε_{Nd} for Haleakala and other Hawaiian volcanoes. L.D. denotes literature data and includes data from the following sources: Cohen and O'Nions (1993), Cohen et al. (1996), Garcia et al. (1992; 1993; 1996; 1998; 2000; 2003), Marske et al. (2008), Pickett and Murrell (1997), Pietruszka and Garcia (1999), Pietruszka et al. (2001; 2006; 2011), Sims et al. (1999). Measured SiO_2 content is plotted and is not corrected for olivine fractionation because samples were picked free of phenocrysts prior to analysis.

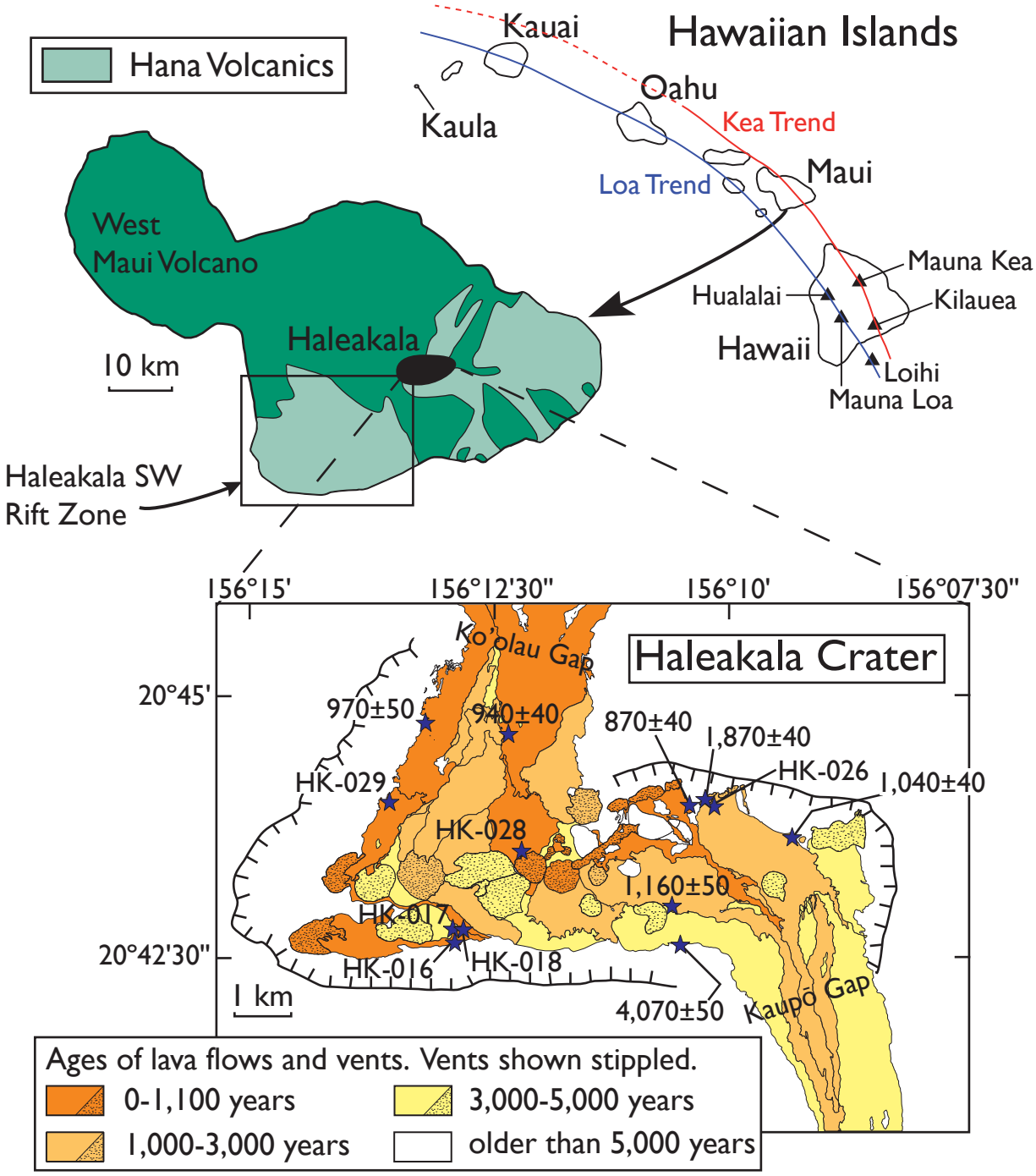
Hana Volcanics
Hawaiian Islands
Kauai
Oahu
Kaula
Kea Trend
Loa Trend
Maui
West
Maui Volcano
Haleakala
10 km
Haleakala SW
Rift Zone
Mauna Kea
Hualalai
Kilauea
Hawaii
Loihi
Mauna Loa
156°15'
156°12'30"
156°10'
156°07'30"
20°45'
20°42'30"
Haleakala Crater
Ko'olau Gap
970±50
940±40
870±40
1,870±40
HK-029
HK-026
1,040±40
HK-028
1,160±50
HK-017
HK-016
HK-018
1 km
4,070±50
Kaupō Gap
Ages of lava flows and vents. Vents shown stippled.
0-1,100 years
1,000-3,000 years
3,000-5,000 years
older than 5,000 years

Figure 1

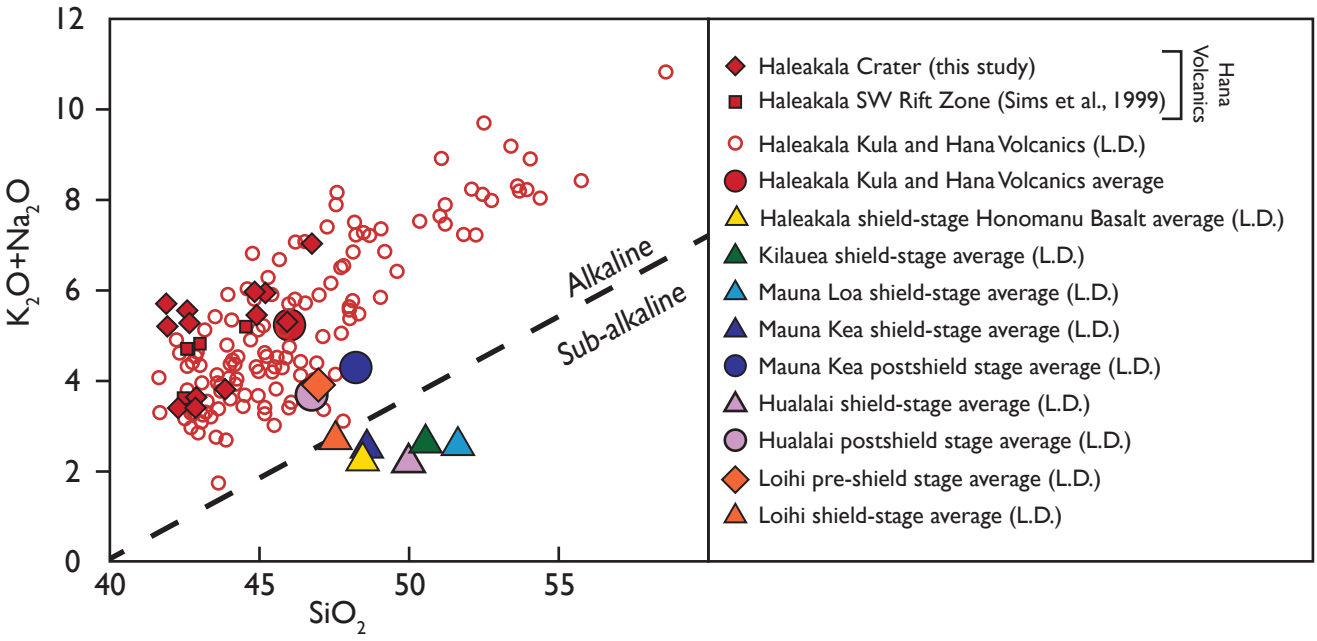
12
10
8
6
4
2
0
40
45
50
55
K_2O+Na_2O
SiO_2
Alkaline
Sub-alkaline
Haleakala Crater (this study)
Haleakala SW Rift Zone (Sims et al., 1999)
Hana Volcanics
Haleakala Kula and Hana Volcanics (L.D.)
Haleakala Kula and Hana Volcanics average
Haleakala shield-stage Honomanu Basalt average (L.D.)
Kilauea shield-stage average (L.D.)
Mauna Loa shield-stage average (L.D.)
Mauna Kea shield-stage average (L.D.)
Mauna Kea postshield stage average (L.D.)
Hualalai shield-stage average (L.D.)
Hualalai postshield stage average (L.D.)
Loihi pre-shield stage average (L.D.)
Loihi shield-stage average (L.D.)

Figure 2

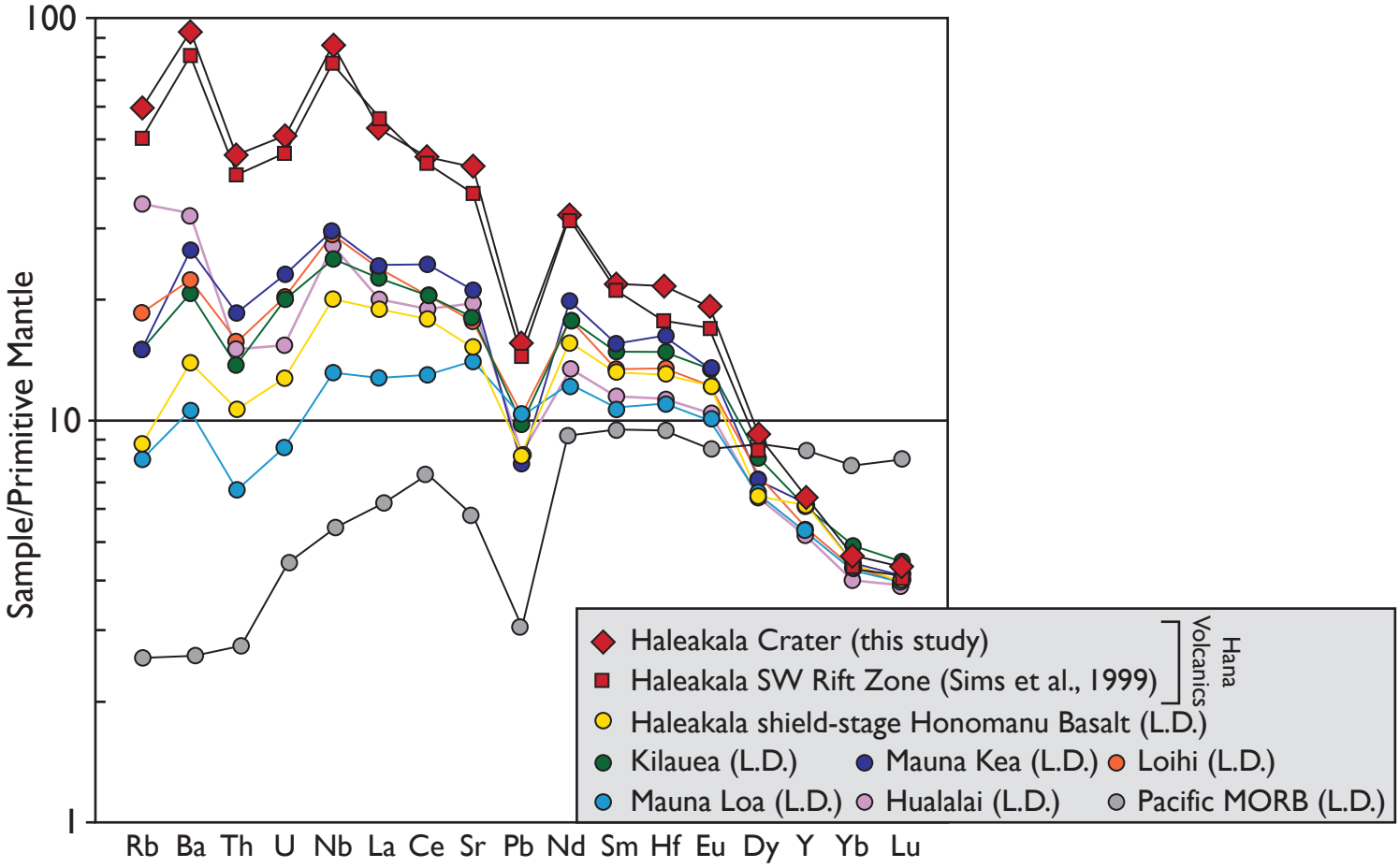
100
10
1
Sample/Primitive Mantle
Rb Ba Th U Nb La Ce Sr Pb Nd Sm Hf Eu Dy Y Yb Lu
Haleakala Crater (this study)
Haleakala SW Rift Zone (Sims et al., 1999)
Hana Volcanics
Haleakala shield-stage Honomanu Basalt (L.D.)
Kilauea (L.D.)
Mauna Kea (L.D.)
Loihi (L.D.)
Mauna Loa (L.D.)
Hualalai (L.D.)
Pacific MORB (L.D.)

Figure 3

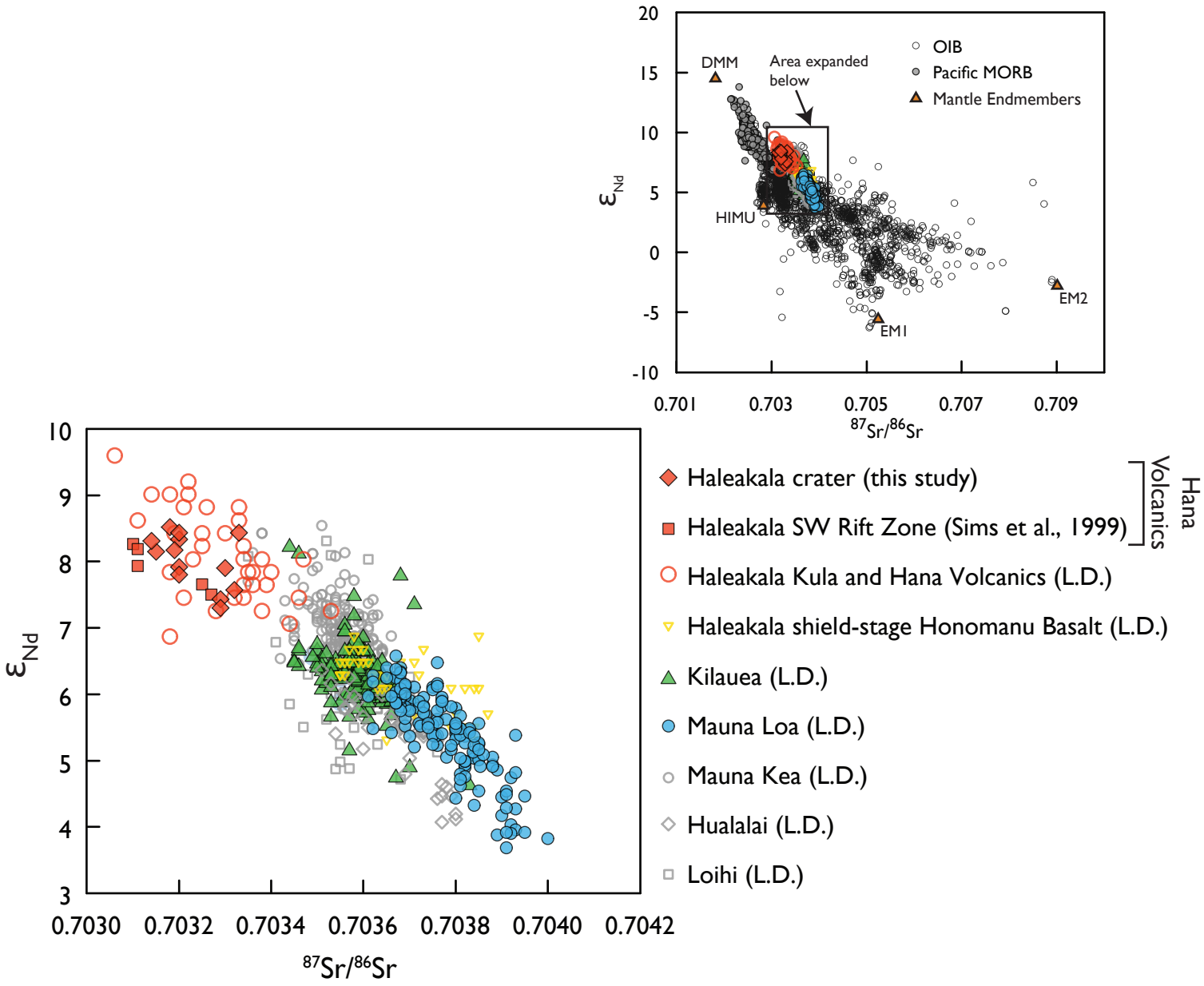
20
15
10
5
0
-5
-10
0.701
0.703
0.705
0.707
0.709
$^{87}Sr/^{86}Sr$
ε_{Nd}
DMM
Area expanded below
HIMU
EM1
EM2
OIB
Pacific MORB
Mantle Endmembers
10
9
8
7
6
5
4
3
0.7030
0.7032
0.7034
0.7036
0.7038
0.7040
0.7042
$^{87}Sr/^{86}Sr$
ε_{Nd}
Haleakala crater (this study)
Haleakala SW Rift Zone (Sims et al., 1999)
Haleakala Kula and Hana Volcanics (L.D.)
Haleakala shield-stage Honomanu Basalt (L.D.)
Kilauea (L.D.)
Mauna Loa (L.D.)
Mauna Kea (L.D.)
Hualalai (L.D.)
Loihi (L.D.)
Hana Volcanics

Figure 4

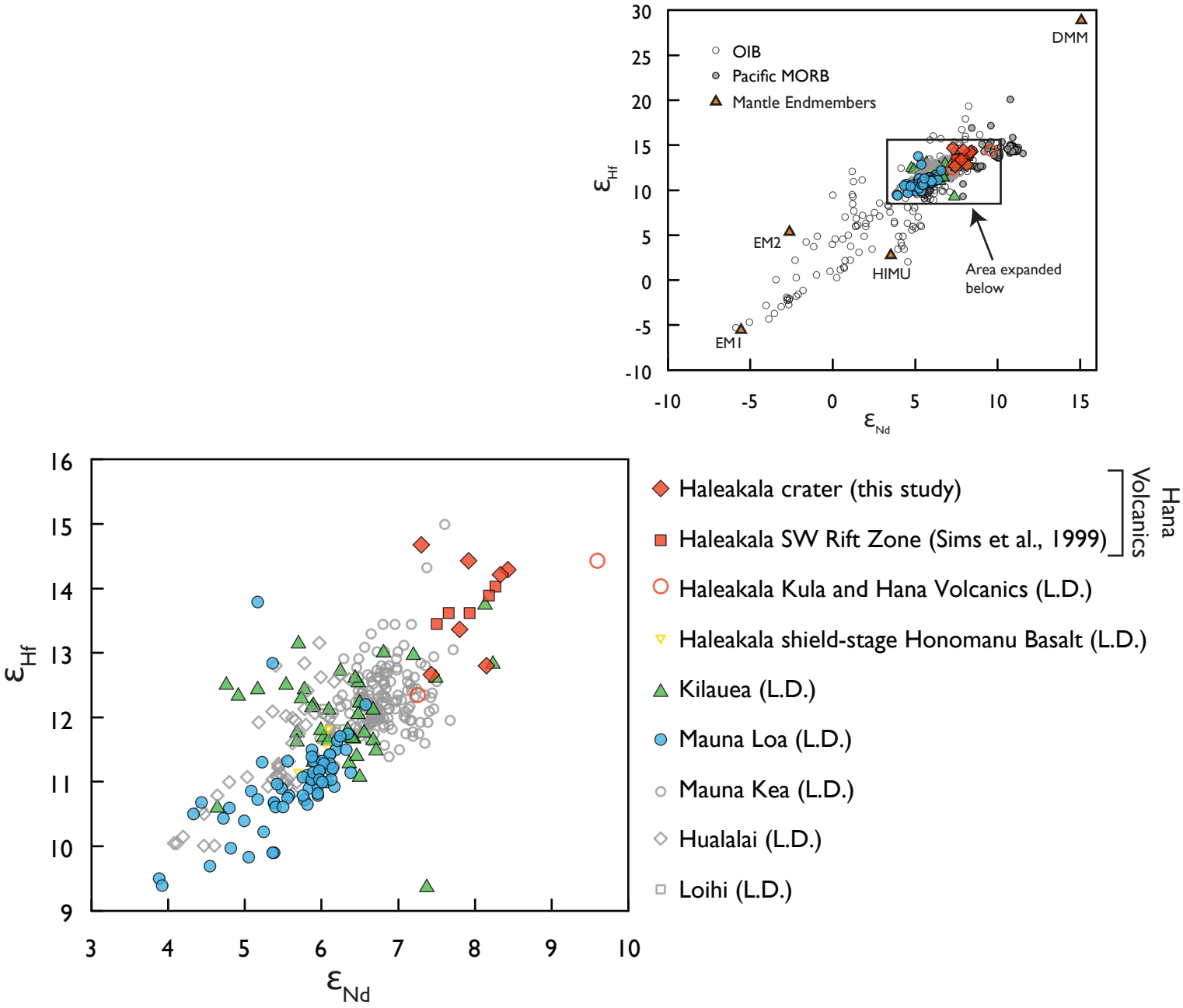
30
25
20
15
10
5
0
-5
-10
-10
-5
0
5
10
15
εHf
εNd
OIB
Pacific MORB
Mantle Endmembers
DMM
EM2
HIMU
EM1
Area expanded
below
16
15
14
13
12
11
10
9
3
4
5
6
7
8
9
10
εHf
εNd
Haleakala crater (this study)
Haleakala SW Rift Zone (Sims et al., 1999)
Haleakala Kula and Hana Volcanics (L.D.)
Haleakala shield-stage Honomanu Basalt (L.D.)
Kilauea (L.D.)
Mauna Loa (L.D.)
Mauna Kea (L.D.)
Hualalai (L.D.)
Loihi (L.D.)
Hana Volcanics

Figure 5

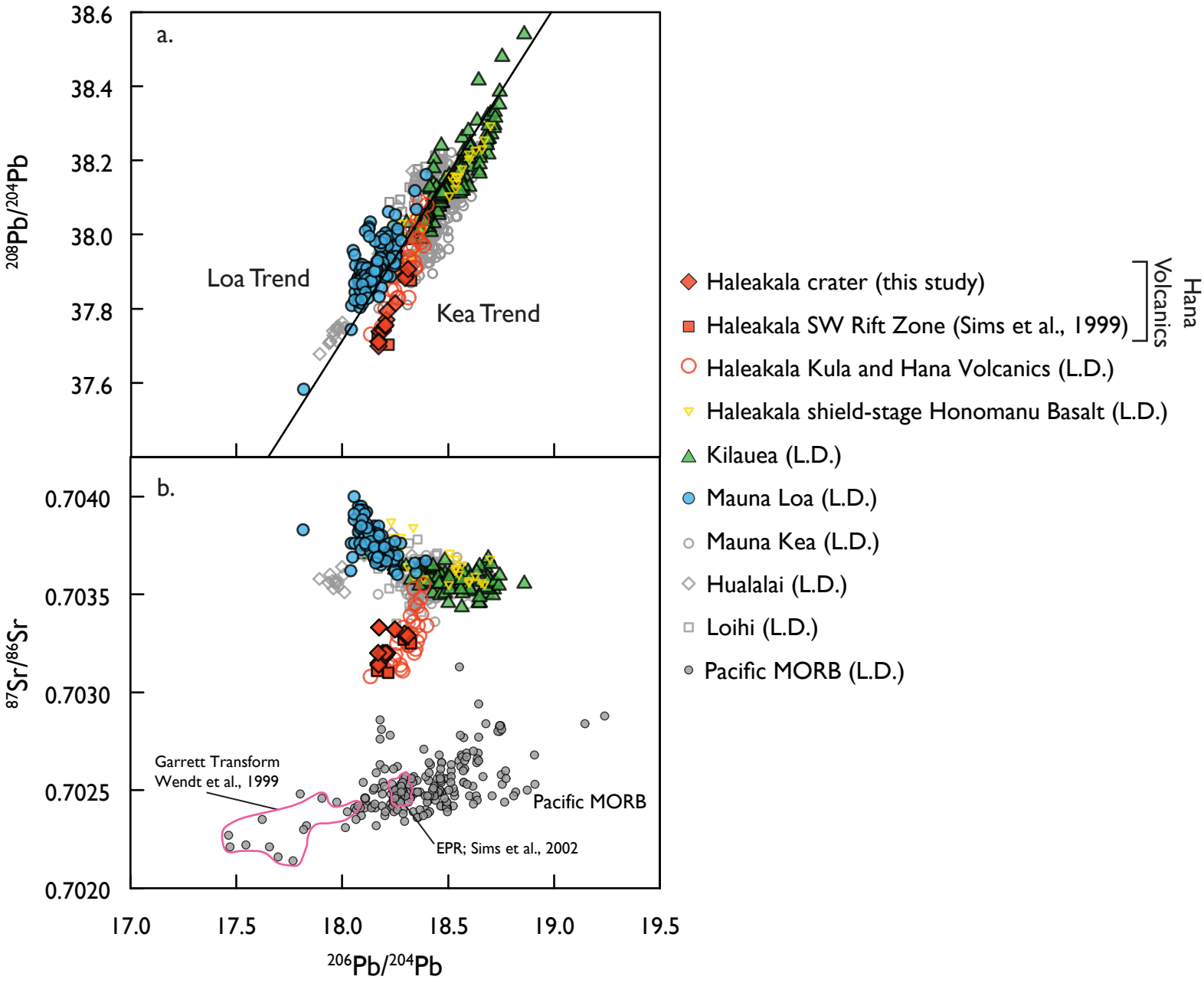
a.
b.
Loa Trend
Kea Trend
Garrett Transform
Wendt et al., 1999
Pacific MORB
EPR; Sims et al., 2002
$^{208}Pb/^{204}Pb$
$^{87}Sr/^{86}Sr$
$^{206}Pb/^{204}Pb$
38.6
38.4
38.2
38.0
37.8
37.6
0.7040
0.7035
0.7030
0.7025
0.7020
17.0
17.5
18.0
18.5
19.0
19.5
Haleakala crater (this study)
Haleakala SW Rift Zone (Sims et al., 1999)
Haleakala Kula and Hana Volcanics (L.D.)
Haleakala shield-stage Honomanu Basalt (L.D.)
Kilauea (L.D.)
Mauna Loa (L.D.)
Mauna Kea (L.D.)
Hualalai (L.D.)
Loihi (L.D.)
Pacific MORB (L.D.)
Hana Volcanics

Figure 6

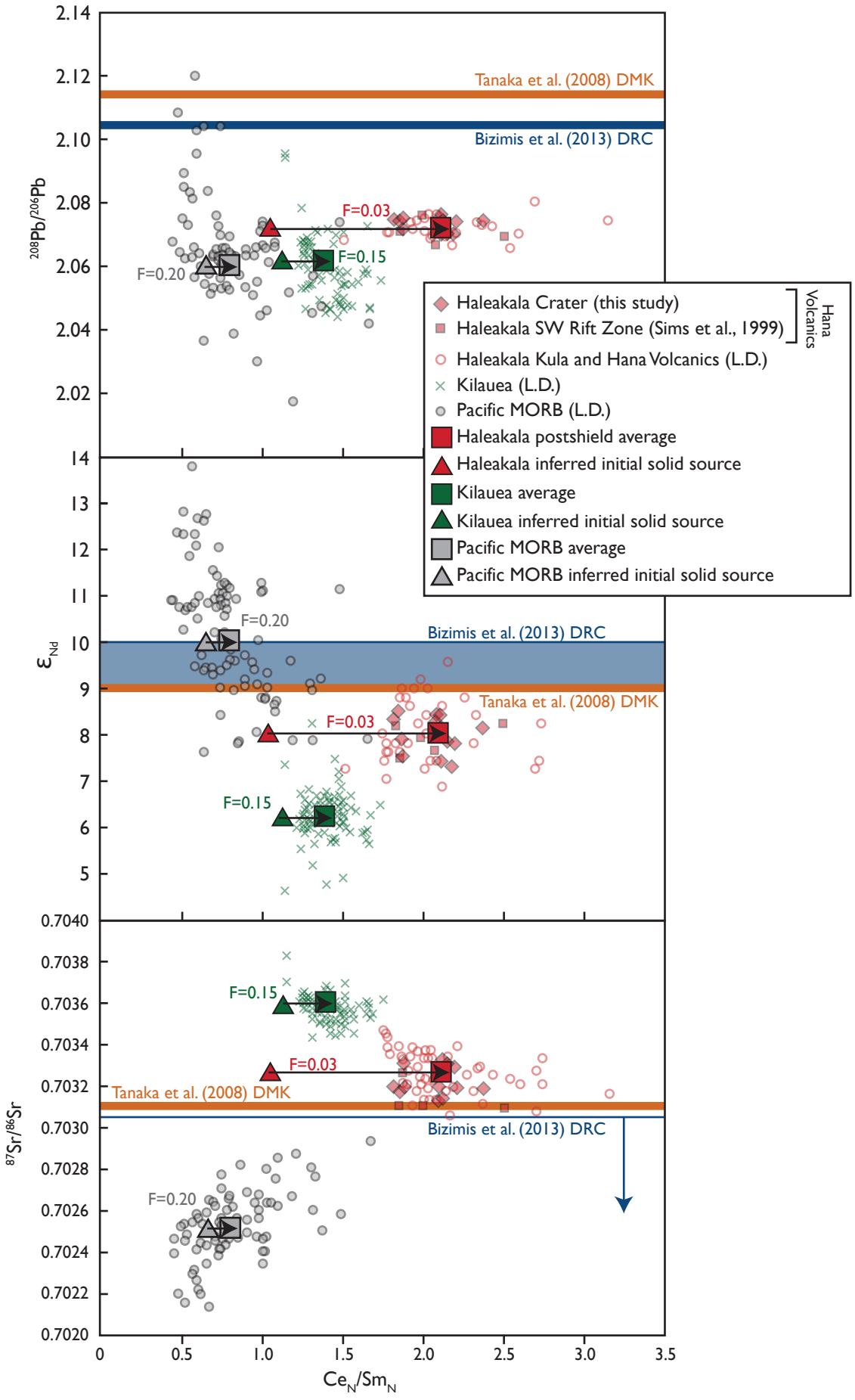
Tanaka et al. (2008) DMK
Bizimis et al. (2013) DRC
F=0.03
F=0.15
F=0.20
Haleakala Crater (this study)
Haleakala SW Rift Zone (Sims et al., 1999)
Hana Volcanics
Haleakala Kula and Hana Volcanics (L.D.)
Kilauea (L.D.)
Pacific MORB (L.D.)
Haleakala postshield average
Haleakala inferred initial solid source
Kilauea average
Kilauea inferred initial solid source
Pacific MORB average
Pacific MORB inferred initial solid source
208Pb/206Pb
εNd
87Sr/86Sr
CeN/SmN

Figure 7

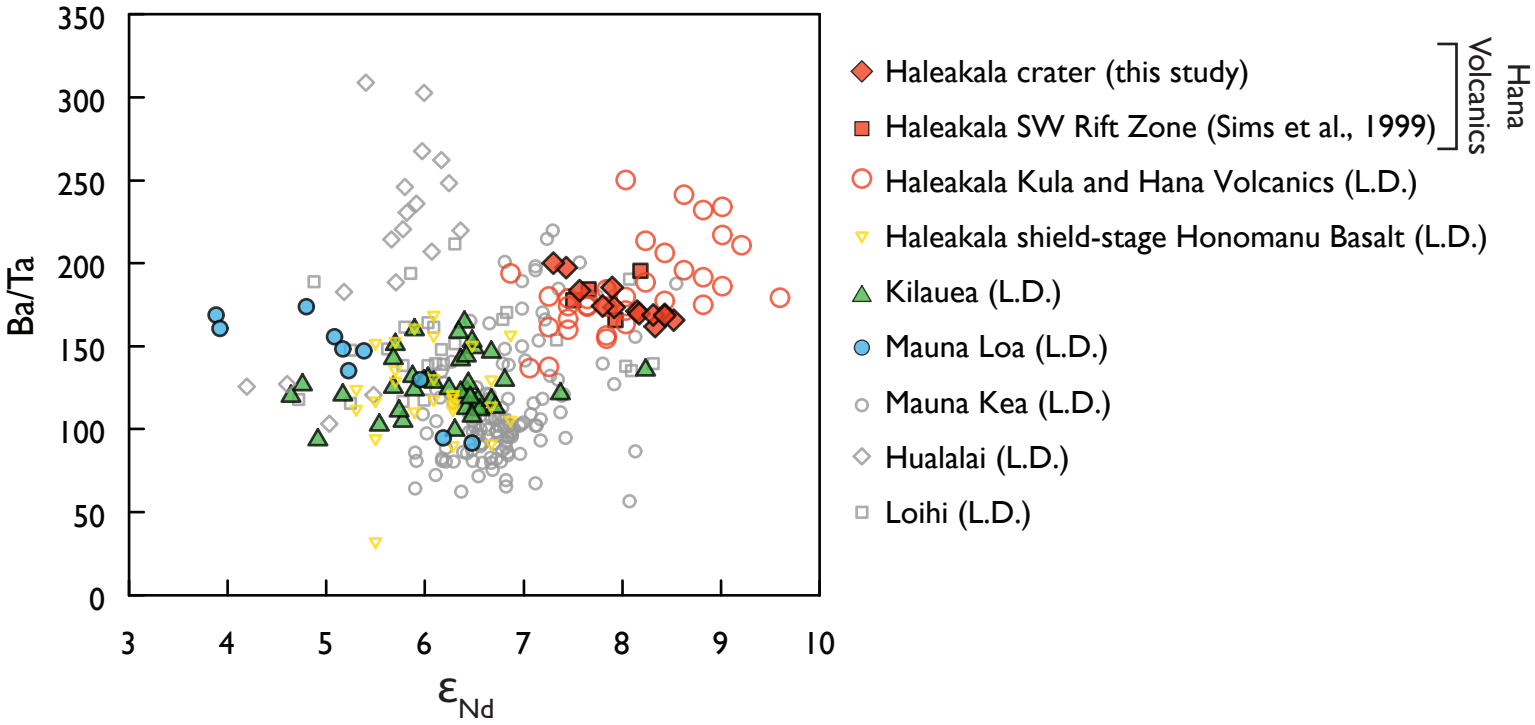
350
300
250
200
150
100
50
0
Ba/Ta
3
4
5
6
7
8
9
10
εNd
Haleakala crater (this study)
Haleakala SW Rift Zone (Sims et al., 1999)
Haleakala Kula and Hana Volcanics (L.D.)
Haleakala shield-stage Honomanu Basalt (L.D.)
Kilauea (L.D.)
Mauna Loa (L.D.)
Mauna Kea (L.D.)
Hualalai (L.D.)
Loihi (L.D.)
Hana Volcanics

Figure 8

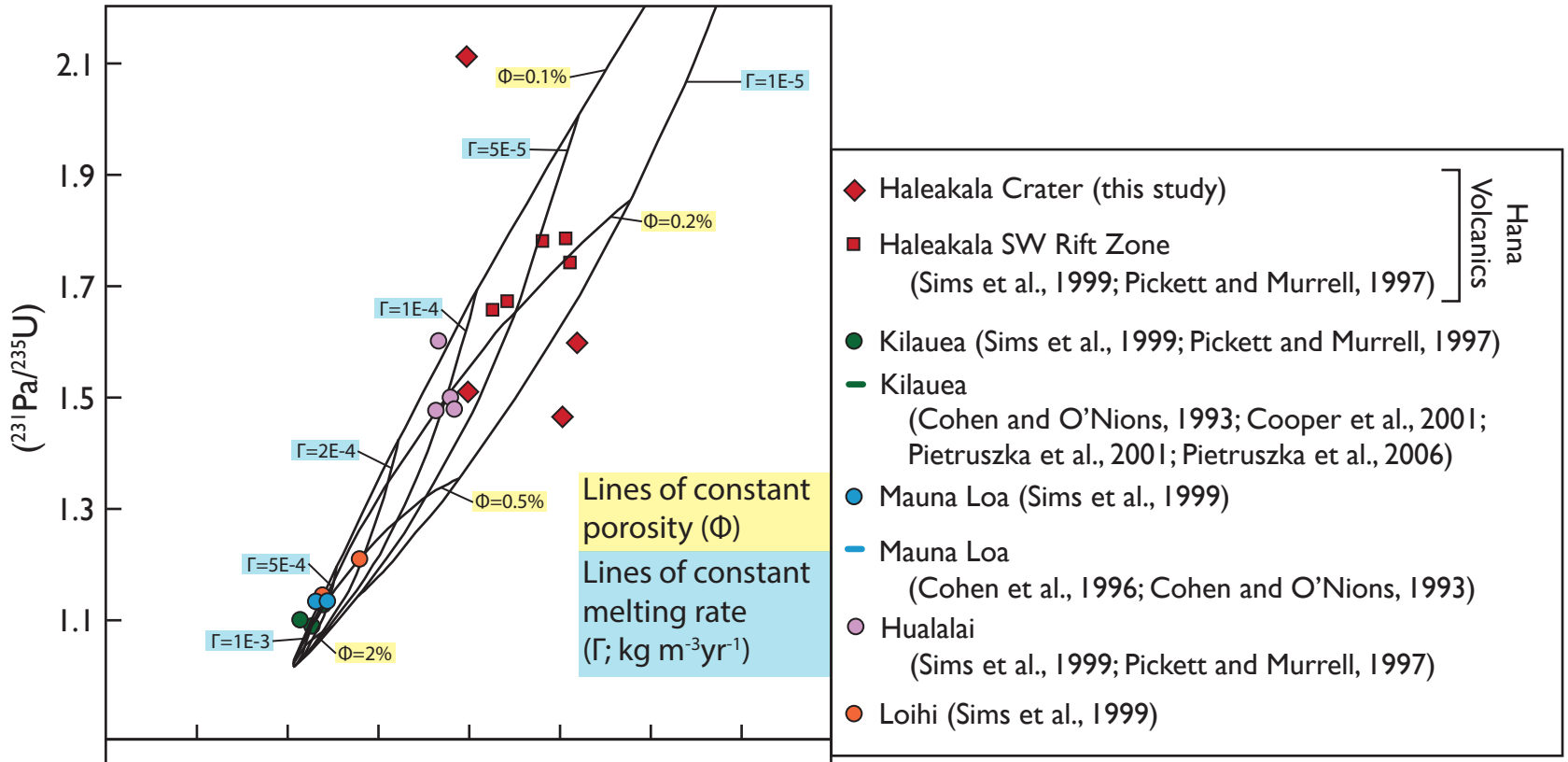
2.1
1.9
1.7
1.5
1.3
1.1
(231Pa/235U)
Φ=0.1%
Γ=1E-5
Γ=5E-5
Φ=0.2%
Γ=1E-4
Γ=2E-4
Φ=0.5%
Γ=5E-4
Γ=1E-3
Φ=2%
Lines of constant porosity (Φ)
Lines of constant melting rate (Γ; kg m-3yr-1)
1.7
1.5
1.3
1.1
0.9
(226Ra/230Th)
0.9
1.0
1.1
1.2
1.3
1.4
1.5
1.6
(230Th/238U)
Haleakala Crater (this study)
Haleakala SW Rift Zone
(Sims et al., 1999; Pickett and Murrell, 1997)
Hana Volcanics
Kilauea (Sims et al., 1999; Pickett and Murrell, 1997)
Kilauea
(Cohen and O'Nions, 1993; Cooper et al., 2001; Pietruszka et al., 2001; Pietruszka et al., 2006)
Mauna Loa (Sims et al., 1999)
Mauna Loa
(Cohen et al., 1996; Cohen and O'Nions, 1993)
Hualalai
(Sims et al., 1999; Pickett and Murrell, 1997)
Loihi (Sims et al., 1999)

Figure 9

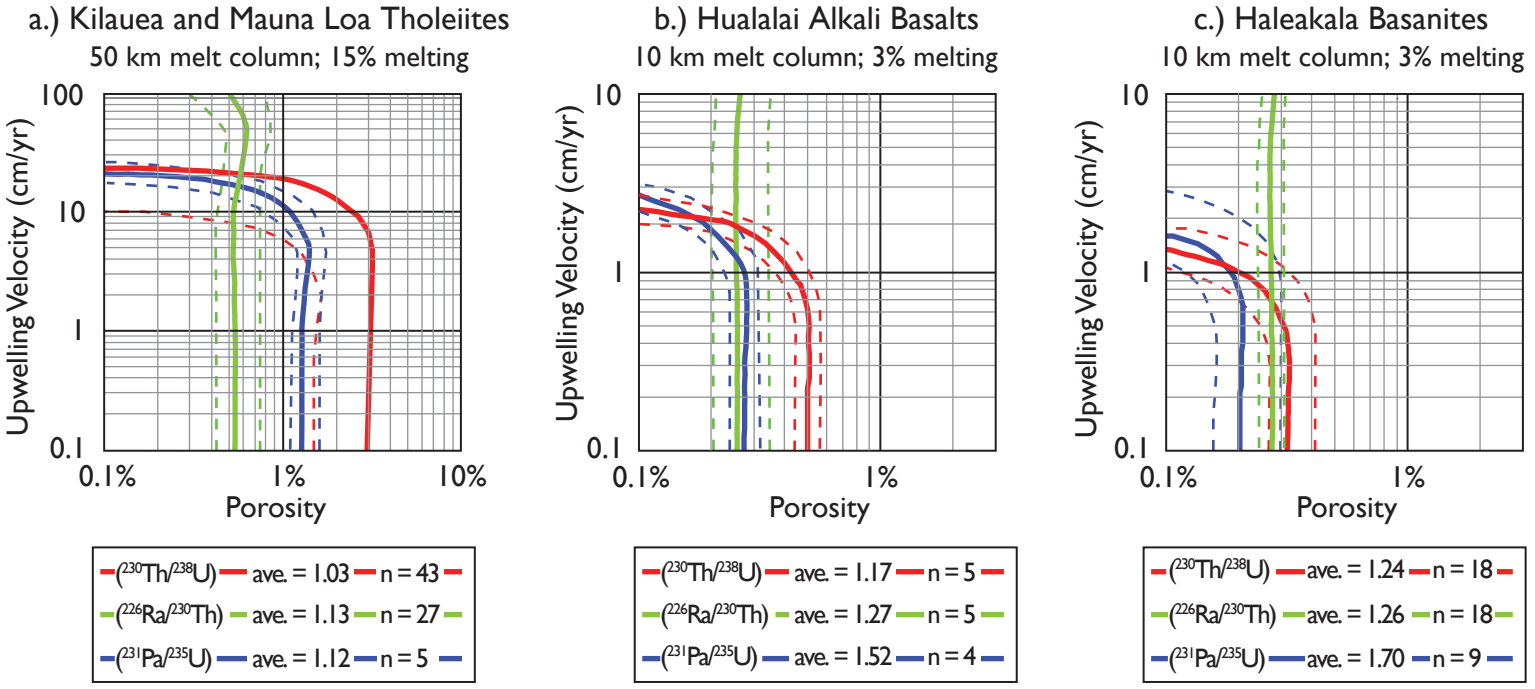
a.) Kilauea and Mauna Loa Tholeiites
50 km melt column; 15% melting
Upwelling Velocity (cm/yr)
100
10
1
0.1
0.1%
1%
10%
Porosity
(230Th/238U) ave. = 1.03 n = 43
(226Ra/230Th) ave. = 1.13 n = 27
(231Pa/235U) ave. = 1.12 n = 5
b.) Hualalai Alkali Basalts
10 km melt column; 3% melting
Upwelling Velocity (cm/yr)
10
1
0.1
0.1%
1%
Porosity
(230Th/238U) ave. = 1.17 n = 5
(226Ra/230Th) ave. = 1.27 n = 5
(231Pa/235U) ave. = 1.52 n = 4
c.) Haleakala Basanites
10 km melt column; 3% melting
Upwelling Velocity (cm/yr)
10
1
0.1
0.1%
1%
Porosity
(230Th/238U) ave. = 1.24 n = 18
(226Ra/230Th) ave. = 1.26 n = 18
(231Pa/235U) ave. = 1.70 n = 9

Figure 10

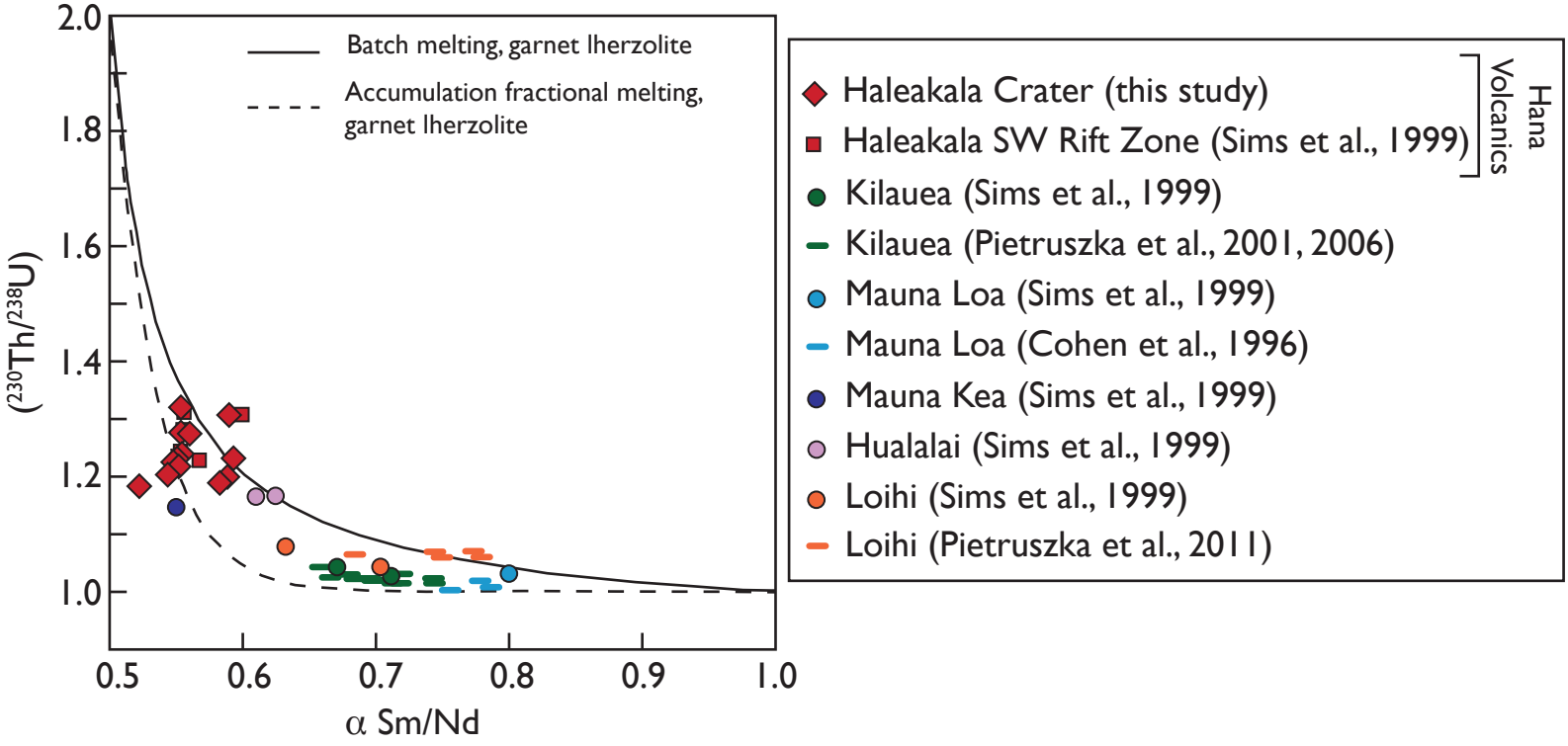
Batch melting, garnet lherzolite
Accumulation fractional melting, garnet lherzolite
(230Th/238U)
α Sm/Nd
2.0
1.8
1.6
1.4
1.2
1.0
0.5
0.6
0.7
0.8
0.9
1.0
Haleakala Crater (this study)
Haleakala SW Rift Zone (Sims et al., 1999)
Hana Volcanics
Kilauea (Sims et al., 1999)
Kilauea (Pietruszka et al., 2001, 2006)
Mauna Loa (Sims et al., 1999)
Mauna Loa (Cohen et al., 1996)
Mauna Kea (Sims et al., 1999)
Hualalai (Sims et al., 1999)
Loihi (Sims et al., 1999)
Loihi (Pietruszka et al., 2011)

Figure 11

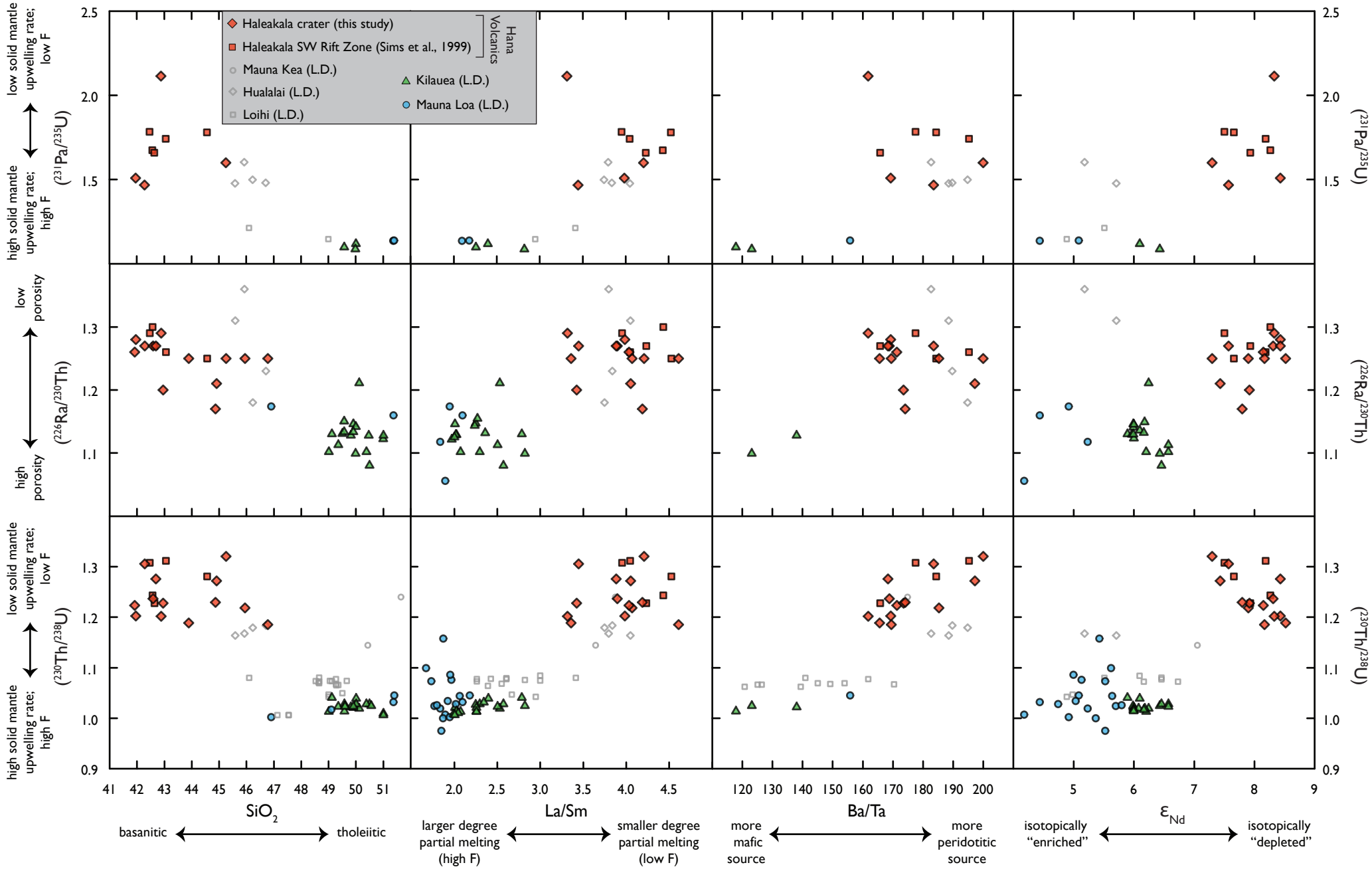
Haleakala crater (this study)
Haleakala SW Rift Zone (Sims et al., 1999)
Hana Volcanics
Mauna Kea (L.D.)
Hualalai (L.D.)
Loihi (L.D.)
Kilauea (L.D.)
Mauna Loa (L.D.)
low solid mantle upwelling rate; low F
high solid mantle upwelling rate; high F
low porosity
high porosity
(231Pa/235U)
(226Ra/230Th)
(230Th/238U)
SiO2
basanitic
tholeiitic
La/Sm
larger degree partial melting (high F)
smaller degree partial melting (low F)
Ba/Ta
more mafic source
more peridotitic source
εNd
isotopically "enriched"
isotopically "depleted"

Figure 12

Table 1: Locations and ages of Haleakala Crater basanite samples.

	Source or flow name	Latitude, N	Longitude, W	Age, in ^{14}C yr B.P.	Reference
HK-16	Sliding Sands lava	20°42.483'	156°12.749'	1000-2000	2
HK-17	Pu‘u o Pele lava	20°42.594'	156°12.745'	~4000	2
HK-18	Ka Lu‘u o ka ‘O‘o lava	20°42.597'	156°12.649'	<970; 800-950	2
HK-19	Pu‘u Maile lava	20°42.455'	156°10.435'	4070±50	1
HK-21	Pu‘u Nole lava	20°42.814'	156°10.568'	1160±50	1
HK-22	Kalua Awa lava	20°43.464'	156°09.286'	1040±40	1
HK-23	Hanakauhi fissure	20°43.790'	156°10.352'	870±40	1
HK-25	Aphyric spatter rampart	20°43.823'	156°10.155'	1870±40	1
HK-26	Kalua Awa lava	20°43.764'	156°10.083'	900-1040	2
HK-28	Halali‘i lava	20°43.342'	156°12.085'	<940	2
HK-29	Youngest Ka Lu‘u o ka ‘O‘o lava	20°43.812'	156°13.426'	<970	2
HK-30	Halali‘i lava	20°44.455'	156°12.219'	940±50	1
HK-31	Ka Lu‘u o ka ‘O‘o lava	20°44.561'	156°13.053'	970±50	1

All samples collected by K. Sims and D. Sherrod, May 1999. Geographic coordinates referable to datum WGS84.

1: ^{14}C age from Sherrod and McGeehin, 1999

2: Age bracketed by stratigraphic relations with dated lava flows, extent of weathering and soil development, and paleomagnetic directions in conjunction with paleosecular variation curve (Sherrod et al., 2006).

Table 2: Major and trace element data for Haleakala Crater basanites.

	HK-16	HK-17	HK-18	HK-19	HK-21	HK-22	HK-23	HK-25	HK-26	HK-28	HK-29	HK-30	HK-31	BHVO-2	BHVO-2	% RSD	BHVO-2 recommended
SiO_2 (wt.%)	44.91	45.95	41.96	45.25	42.28	42.88	41.91	46.78	43.89	42.95	42.59	44.87	42.69	50.09	50.34	0.4%	49.9 ± 0.6
TiO_2	3.61	3.23	3.94	3.40	3.20	3.29	4.01	2.87	3.38	3.38	3.92	3.13	3.86	2.70	2.69	0.2%	2.73 ± 0.04
Al_2O_3	16.64	16.38	14.03	16.49	12.39	12.65	14.75	17.59	12.90	13.05	13.79	15.55	13.86	13.56	13.54	0.1%	13.5 ± 0.2
Fe_2O_3	14.45	14.05	15.88	13.88	15.88	15.11	16.06	12.24	15.17	15.20	15.78	13.65	15.55	12.41	12.35	0.3%	12.3 ± 0.2
MnO	0.20	0.20	0.21	0.20	0.19	0.19	0.22	0.22	0.19	0.19	0.21	0.21	0.21	0.16	0.16	0.0%	0.13 ± 0.004
MgO	5.46	5.94	6.90	5.08	10.61	9.34	6.01	3.65	8.77	9.49	6.83	6.01	6.88	7.27	7.27	0.0%	7.23 ± 0.12
CaO	8.99	9.93	11.29	8.59	11.94	11.95	10.12	7.73	11.98	11.97	11.15	9.43	11.24	11.38	11.32	0.4%	11.4 ± 0.2
Na_2O	4.05	3.90	3.76	4.36	2.53	2.63	4.09	5.13	2.87	2.73	3.94	4.27	3.73	2.35	2.24	3.3%	2.22 ± 0.08
K_2O	1.41	1.39	1.43	1.58	0.88	0.82	1.61	1.88	0.93	0.93	1.56	1.65	1.53	0.54	0.53	0.7%	0.52 ± 0.01
P_2O_5	0.57	0.58	0.58	0.58	0.37	0.37	0.64	0.82	0.39	0.38	0.58	0.64	0.56	0.27	0.27	0.4%	0.27 ± 0.02
Total	100.29	101.54	100.00	99.42	100.27	99.23	99.41	98.90	100.48	100.28	100.35	99.40	100.12	100.73	100.72		
$H2O^-$	1.22	1.14	0.35	0.39	0.78	0.72	0.68	1.23	0.19	0.48	0.01	0.91	0.93		0.776		
LOI	0.10	0.20	-0.25	-0.29	-0.64	-0.63	-0.20	0.15	-0.05	-0.15	-0.01	-1.09	-1.23		-0.460		
Li (ppm)	8.14	7.73	7.21	8.66	5.28	5.52	8.11	10.57	6.14	5.80	7.40	8.91	7.38	4.76	4.89	1.9%	5
Be	2.12	2.09	2.08	2.07	1.35	1.45	2.34	3.03	1.53	1.54	2.21	2.41	2.22	1.25	1.24	0.5%	
Sc	15.9	18.0	20.7	14.7	29.4	28.2	16.4	7.46	28.2	28.3	21.1	15.8	22.4	31.1	30.9	0.5%	32 ± 1
Ni	15.0	44.3	63.5	8.53	128	144	34.4	0.60	134	113	62.2	51.8	65.6	115	116	0.1%	119 ± 7
Cu	40.8	49.3	81.4	36.1	42.8	71.0	49.4	15.7	75.3	45.6	82.9	39.0	86.0	139	139	0.1%	127 ± 7
Ga corr	23.8	24.4	26.7	23.9	21.9	22.7	27.5	27.4	24.1	22.7	26.6	25.7	27.1	21.0	20.4	2.1%	21.7 ± 0.9
Cr	2.38	109	21.3	2.17	420	408	6.49	1.01	402	395	23.9	145	65.4	284	284	0.0%	280 ± 19
Co	39.2	39.8	51.8	35.5	61.4	57.5	49.7	23.6	55.2	54.9	52.9	40.7	53.1	44.8	44.1	1.2%	45 ± 3
Y	30.8	29.9	28.5	30.6	24.1	23.9	29.7	33.0	25.3	25.0	28.2	30.8	29.0	26.5	26.6	0.1%	26 ± 2
Zr	249	242	268	257	190	191	280	330	200	191	269	277	275	185	182	0.9%	172 ± 11
V	243	260	386	215	386	385	371	126	403	380	388	252	399	307	308	0.1%	317 ± 11
Nb	60.6	58.3	61.3	63.1	37.7	37.9	67.2	77.7	40.5	40.0	62.3	63.8	63.0	19.5	19.4	0.5%	18 ± 2
Cs	0.42	0.40	0.39	0.38	0.20	0.24	0.42	0.56	0.27	0.28	0.38	0.45	0.39	0.11	0.10	5.1%	
Zn corr	113	107	116	103	103	98.4	124	117	103	100	118	117	116	94.9	94.0	0.7%	103 ± 6
Ba	726	646	635	761	424	388	708	806	423	431	650	676	659	135	133	0.7%	130 ± 13
Rb	37.7	38.0	38.4	42.0	23.5	23.0	42.5	52.4	26.3	26.7	38.3	42.8	40.4	10.7	10.7	0.0%	9.8 ± 1.0
Sr	1005	912	902	1013	591	599	977	1059	629	610	905	933	920	397	395	0.4%	389 ± 23

Pb	2.99	2.55	2.57	2.95	1.47	1.51	2.76	2.49	1.59	1.49	2.58	2.75	2.60	1.63	1.61	1.1%	
Th	3.85	3.68	3.73	3.97	2.47	2.45	4.19	5.41	2.62	2.57	3.89	4.25	3.97	1.24	1.27	1.6%	1.2 ± 0.3
U	1.07	1.06	1.10	1.06	0.69	0.72	1.21	1.59	0.77	0.74	1.12	1.22	1.11	0.43	0.43	0.1%	
La	36.4	35.3	37.8	37.4	24.5	23.7	40.5	49.2	25.4	24.9	37.6	39.8	38.2	14.6	14.7	0.8%	15 ± 1
Ce	78.8	77.1	83.1	80.5	55.0	54.1	88.0	105	57.9	56.5	83.4	86.5	85.4	37.4	37.8	0.7%	38 ± 2
Pr	10.1	9.84	10.7	10.2	7.28	7.19	11.3	13.0	7.68	7.42	10.8	11.1	11.0	5.40	5.45	0.6%	
Nd	41.9	40.7	44.7	42.0	31.3	31.2	47.2	52.5	33.2	31.8	44.7	44.8	45.4	24.8	24.9	0.3%	25.0 ± 1.8
Sm	8.98	8.68	9.50	8.90	7.10	7.15	10.1	10.7	7.57	7.29	9.65	9.51	9.84	6.13	6.09	0.4%	6.2 ± 0.4
Eu	3.05	2.90	3.12	3.02	2.36	2.38	3.30	3.49	2.52	2.43	3.18	3.17	3.26	2.04	2.05	0.2%	
Gd	8.51	8.19	8.85	8.43	6.88	6.91	9.20	9.65	7.29	7.13	8.89	8.88	9.15	6.29	6.36	0.8%	6.3 ± 0.2
Tb	1.28	1.23	1.30	1.27	1.04	1.04	1.36	1.43	1.09	1.07	1.33	1.34	1.36	1.00	1.00	0.1%	0.9
Dy	6.55	6.29	6.38	6.47	5.30	5.33	6.70	7.14	5.59	5.51	6.46	6.65	6.60	5.40	5.46	0.9%	
Ho	1.19	1.14	1.11	1.18	0.95	0.94	1.18	1.28	0.99	0.98	1.12	1.20	1.15	1.01	1.03	1.0%	1.04 ± 0.04
Er	2.96	2.82	2.64	2.94	2.28	2.27	2.82	3.17	2.40	2.37	2.67	2.98	2.77	2.53	2.55	0.4%	
Yb	2.34	2.23	1.92	2.36	1.72	1.71	2.08	2.49	1.79	1.79	1.93	2.26	1.98	2.07	2.04	0.9%	2.0 ± 0.2
Lu	0.34	0.32	0.27	0.34	0.25	0.24	0.30	0.36	0.26	0.26	0.27	0.33	0.28	0.30	0.29	0.5%	0.28 ± 0.01
Hf	6.07	5.83	6.55	6.13	5.01	5.10	6.88	7.37	5.34	5.04	6.72	6.48	6.82	4.69	4.78	1.3%	4.1 ± 0.3
Ta	3.68	3.49	3.75	3.80	2.31	2.40	4.14	4.76	2.56	2.49	3.85	3.88	3.91	1.28	1.28	0.2%	1.4

Major elements analyzed by ICP-OES at Boston University. Trace elements analyzed by VG PQ ExCell quadrupole ICP-MS at Boston University following the procedures of Kelley et al. (2003).

Each sample solution was analyzed twice in the run, and the average relative standard deviation (RSD) for all elements was 1.5%. USGS rock standard BHVO-2 was analyzed twice as an unknown for quality control.

The inter-run precision can be assessed from the difference in BHVO-2 in the two runs and is generally better than 2% relative standard deviation (RSD).

This precision is typical of that obtained in comparable analyses over several years in the Boston University lab. USGS recommended values of BHVO-2 are shown for comparison.

Table 3: Sr, Nd, Hf, and Pb isotopic data for Hana Volcanics samples.

	$^{87}Sr/^{86}Sr$[a,g]	$^{143}Nd/^{144}Nd$[b,g]	ε_{Nd}[c]	$^{176}Hf/^{177}Hf$[d]	ε_{Hf}[e]	$^{206}Pb/^{204}Pb$[f,g]	$^{207}Pb/^{204}Pb$[f,g]	$^{208}Pb/^{204}Pb$[f,g]
Haleakala Crater:								
HK-16	0.703291	0.513019	7.4	0.283130	12.7	18.299	15.464	37.889
HK-17	0.703298	0.513043	7.9			18.295	15.461	37.882
HK-18	0.703331	0.513070	8.4	0.283176	14.3	18.174	15.445	37.738
HK-19	0.703292	0.513012	7.3	0.283187	14.7	18.310	15.460	37.907
HK-21	0.703324	0.513026	7.6			18.248	15.452	37.814
HK-22	0.703202	0.513065	8.3	0.283174	14.2	18.192	15.443	37.742
HK-23	0.703145	0.513056	8.2	0.283134	12.8	18.171	15.434	37.699
HK-25	0.703191	0.513057	8.2			18.206	15.449	37.770
HK-26	0.703183	0.513075	8.5			18.199	15.447	37.754
HK-28	0.703204	0.513044	7.9	0.283180	14.4	18.213	15.450	37.793
HK-29	0.703140	0.513064	8.3			18.171	15.440	37.712
HK-30	0.703195	0.513038	7.8	0.283150	13.4	18.203	15.444	37.756
HK-31	0.703199	0.513070	8.4			18.170	15.438	37.710
Haleakala Southwest Rift Zone (SWRZ; Sims et al., 1995; 1999; Stracke et al., 1999)[h]:								
HK-02	0.70325	0.512228	7.7	0.283157	13.6	18.324	15.464	37.876
HK-04	0.70327	0.512220	7.5	0.283152	13.5	18.291	15.470	37.887
HK-06	0.70310	0.512259	8.3	0.283169	14.0	18.216	15.432	37.702
HK-10	0.70311	0.512242	7.9	0.283157	13.6	18.166	15.440	37.722
HK-11	0.70310	0.512255	8.2	0.283165	13.9			

[a]Sr isotopes measured at WHOI using a Thermo Fisher Neptune MC-ICP-MS. Isotopic ratios normalized for instrumental mass fractionation relative to $^{86}Sr/^{88}Sr$=0.1194. Results normalized to NBS987=0.710240. Internal precision for Sr was 5-10 ppm (2σ); external precision was estimated at <30 ppm (2σ). Total procedural blanks for Sr were <400 pg. Average measured value for NBS987 was 0.710244 ± 0.000030 (2σ).

[b]Nd isotopes measured at WHOI using a Thermo Fisher Neptune MC-ICP-MS. Isotopic ratios normalized for instrumental mass fractionation relative to $^{146}Nd/^{144}Nd$=0.7219. Results normalized to LaJolla=0.511847. Internal precision for Nd was 5-10 ppm (2σ); external precision estimated at <30 ppm (2σ). Total procedural blanks were <100 pg. Average measured value for LaJolla was 0.511825 ± 0.000008 (2σ).

[c]ε_{Nd} for Haleakala Crater samples calculated using ε_{Nd}(CHUR)=0.512638.

[d]Hf isotopes measured using the Lamont Isolab 54 Secondary Ionization mass spectrometer (England et al., 1992) at the National high Magnetic Field Laboratory. JMC-475 was used as a standard and the long term average for this standard of 0.2822 for $^{176}Hf/^{177}Hf$ was also obtained in this study. Hf isotope ratios are corrected to 0.282165 for JMC-475. External precision for Hf estimated at <30 ppm (2σ). Total procedural blanks were <30 pg.

[e]ε_{Hf} calculated using ε_{Hf}(CHUR)=0.282772.

[f]Pb isotopes measured at WHOI using a Thermo Fisher Neptune MC-ICP-MS. Pb isotope compositions were normalized for instrumental mass bias relative to NBS/SRM 997 $^{203}Tl/^{205}Tl = 0.41891$. NBS981 was analyzed as a bracketing standard (White et al., 2000); the following values for NBS981 from Todt et al. (1996) were used for normalization: $^{206}Pb/^{204}Pb = 16.9356$, $^{207}Pb/^{204}Pb = 15.4891$, and $^{208}Pb/^{204}Pb = 36.7006$. The internal precision of Pb isotopic ratios (xxx/204) was 15-60 ppm. External reproducibility ranged from 75 ppm (2σ) for $^{207}Pb/^{206}Pb$ to 200 ppm (2σ) for $^{208}Pb/^{204}Pb$. The total procedural blank was 120-150 pg. Analyses of USGS standards AGV-1 gave $^{206}Pb/^{204}Pb=18.9414$, $^{207}Pb/^{204}Pb=15.6548$, and $^{208}Pb/^{204}Pb=38.5615$ and for BCR-1 $^{206}Pb/^{204}Pb=18.8215$, $^{207}Pb/^{204}Pb=15.6356$, and $^{208}Pb/^{204}Pb=38.7309$.

[g]See Hart et al. (2004, 2005) and Hart and Blusztajn (2006) for further details on Sr, Nd, and Pb isotopic methods.

[h]Nd and Sr isotopes for Haleakala SWRZ samples reported in Sims et al. (1995; 1999). ε_{Nd} calculated using ε_{Nd}(CHUR)=0.511836. These were measured at UC Berkeley and normalized to $^{146}Nd/^{142}Nd=0.636151$. Hf isotopes for SWRZ samples reported in Stracke et al. (1999).

Table 4: U-series data for Hana Volcanics samples.[a,b,c]

	[Th] µg/g[e]	[U] µg/g[e]	[^{226}Ra] fg/g[f]	[^{231}Pa] fg/g[g]	^{230}Th/^{232}Th (x 10^{-6}) ± 2σ RSE (%)	(^{230}Th/^{232}Th)[d]	(^{230}Th/^{238}U)[d]	(^{226}Ra/^{230}Th)$_{measured}$	(^{226}Ra/^{230}Th)$_{age\ corr.}$	(^{231}Pa/^{235}U)	[^{227}Ac] fg/g[h]	(^{227}Ac/^{231}Pa)
Haleakala Crater:												
HK-16	3.85	1.07	510		5.773 ± 0.1%	1.069	1.267	1.113	1.213			
HK-17	3.68	1.06	454		5.731 ± 0.1%	1.061	1.214	1.046	1.253			
HK-18	3.73	1.10	530	542	5.806 ± 0.1%	1.075	1.197	1.188	1.283	1.509	0.36	1.02[i]
HK-19	3.97	1.06	492	552	5.756 ± 0.1%	1.065	1.315	1.045	1.252	1.599	0.36	1.00[i]
HK-21	2.47	0.69	351	327	5.922 ± 0.1%	1.096	1.301	1.167	1.273	1.466	0.21	0.99[i]
HK-22	2.45	0.72	342	493	5.724 ± 0.2%	1.059	1.197	1.184	1.287	2.115	0.33	1.03
HK-23	4.19	1.21	587		5.763 ± 0.1%	1.067	1.218	1.179	1.259			
HK-25	5.41	1.59	707		5.708 ± 0.1%	1.057	1.181	1.113	1.250			
HK-26	2.62	0.77	358		5.705 ± 0.1%	1.056	1.184	1.165	1.250			
HK-28	2.57	0.74	347		5.772 ± 0.2%	1.068	1.222	1.137	1.204			
HK-29	3.89	1.12	551		5.826 ± 0.1%	1.078	1.231	1.180	1.271			
HK-30	4.25	1.22	560		5.759 ± 0.1%	1.066	1.224	1.111	1.165			
HK-31	3.97	1.11	560		5.826 ± 0.1%	1.078	1.271	1.177	1.268			
Standards[j]:												
ATHO	7.44	2.26	844		5.495 ± 0.1%	1.015	1.104	1.003				
TML	30.50	10.79	3604		5.820 ± 0.2%	1.070	0.998	0.989				
BCR-2	5.89	1.71	565	555	4.740 ± 0.2%	0.874	0.992	0.986		0.997	0.36	0.99
BHVO-1				163							0.11	1.02

[a]Parentheses denote activity

[b]λ238=1.551x10^{-10} yr^{-1}; λ232=4.948x$10^{-11}$$yr^{-1}$; λ226=4.331x$10^{-4}$$yr^{-1}$; λ231=2.115x$10^{-5}$$yr^{-1}$; λ235=9.8485x$10^{-10}$$yr^{-1}$ (Jaffey et al., 1971; Le Roux and Glendenin, 1963; Holden, 1990; Tuli, 2000; Robert et al., 1969). 2σ total errors are <2.2% for [U], <1.6% for [Th], <3.5% for [Ra] and <2.4% for [Pa]. These errors include uncertainties in spike calibrations as well as measurement error and uncertainty in standards against which instrument measurements were calibrated. These errors do not include uncertainties in λ238 (0.07%), λ232 (0.5%), λ226 (0.4%), λ231 (0.04%) or λ235 (0.07%).

[c]Activity ratios calculated using λ230=9.158x$10^{-6}$$yr^{-1}$ (Cheng et al., 2000) and λ232=4.948x$10^{-11}$$yr^{-1}$ (Le Roux and Glendenin, 1963). 2σ errors range from 0.4% to 1% and do not include uncertainties in λ230 (0.4%) or λ232 (0.5%).

[d]Isotopic compositions were measured with a Thermo Fisher Neptune MC-ICP-MS at WHOI. ^{232}Th and ^{238}U were measured on a Faraday cup and ^{230}Th on an axial, discrete dynode ion counter with a repelling potential quadrupole (RPQ). Abundance sensitivity over 2 AMU at 85% transmission was ~50 ppb. An exponential correction was used to correct for the tailing of ^{232}Th on ^{230}Th. Use of UCSC Th 'A' for Th-bracketing results in inter-day reproducibility of 0.4-1.5% (2σ). ^{236}U/^{238}U ratios of U010 were measured to correct for mass bias drift and to calibrate SEM yield. Standard-sample-standard bracketing was used for uranium analyses.

[e]U and Th concentrations were measured by isotope dilution using a Thermo Fisher Element 2 high resolution sector-field ICP-MS at WHOI. Mass fractionation was corrected by sample-standard bracketing with NBL-112A, using a linear interpolation of ^{235}U/^{238}U measurements of the standard.

[f] ^{226}Ra concentrations were analyzed by isotope dilution mass spectrometry at WHOI with a Thermo Fisher Neptune MC-ICP-MS. Aliquots were spiked with ^{228}Ra to attain ^{226}Ra/^{228}Ra ≈ 10. Measurement errors do not include the uncertainty in λ226, which is 0.4%.

[g] ^{231}Pa concentrations were measured by isotope dilution on a Thermo Fisher Element 2 at WHOI. Mass fractionation was monitored by sample-standard bracketing

with NBS 960.

[h]A value of 20.0 dpm/g was obtained for IAEA liquid standard (certified value of 19.5 dpm/g).

[i]($^{227}Ac/^{231}Pa$) is an average of 2 analyses of HK-18 (1.025; 1.011), of 2 analyses for HK-19 (0.996; 0.996), and of 4 analyses for HK-21 (2σ SD=0.042).

[j]ATHO, TML, and BCR-2 rock standards were measured at WHOI in replicate (N) for quality assurance by MC-ICP-MS over the same time interval as the Haleakala Crater samples analyzed in this study. Averages of replicate measurements are shown in the table. For ATHO, N=8 for [Th], [U], ($^{230}Th/^{232}Th$), and ($^{230}Th/^{238}U$); N=15 for measured $^{230}Th/^{232}Th$; N=3 for [Ra] and ($^{226}Ra/^{230}Th$). For TML N=12 for [Th], [U], ($^{230}Th/^{232}Th$), and ($^{230}Th/^{238}U$); N=15 for measured $^{230}Th/^{232}Th$; N=5 for [Ra] and ($^{226}Ra/^{230}Th$). For BCR-2, N=6 for [Th], [U], ($^{230}Th/^{232}Th$) and ($^{230}Th/^{238}U$); N=10 for measured $^{230}Th/^{232}Th$; N=6 for [Ra] and ($^{226}Ra/^{230}Th$). Sims et al. (2008b) compare analyses of synthetic and rock standards analyzed at WHOI with those of other laboratories.

($^{227}Ac/^{231}Pa$) for BHVO-1 is average of 3 analyses (2σ SD=0.088).

Table 5: Summary of solid mantle upwelling velocities and porosity from contour plots generated with chromatographic porous flow model (Spiegelman, 2000) using four different sets of D values for U and Th. D values for Ra and Pa from Lundstrom et al. (1994) were used for all models.

	Tholeiites (Kilauea and Mauna Loa) 50 km melt column; 15% melting	Alkali basalts (Hualalai) 10 km melt column; 3% melting	Basanites (Haleakala) 10 km melt column; 3% melting
Inverted D values (Sims et al., 1999)			
garnet peridotite			
Maximum porosity	0.5-0.6%	0.2-0.3%	0.1-0.3%
Solid mantle upwelling velocity	10-20 cm/yr	1-2 cm/yr	0.7-1.0 cm/yr
Salters and Longhi, 1999			
garnet peridotite			
Maximum porosity	2-3%	1-2%	1-2%
Solid mantle upwelling velocity	50-80 cm/yr	2-4 cm/yr	1-2 cm/yr
Lundstrom et al., 1994			
garnet peridotite			
Maximum porosity	1-2%	0.5-0.7%	no convergence
Solid mantle upwelling velocity	20-30 cm/yr	1-2 cm/yr	no convergence
Elkins et al., 2008			
garnet pyroxenite			
Maximum porosity	5-7% to no convergence*	no convergence	no convergence
Solid mantle upwelling velocity	90-200 cm/yr to no convergence*	no convergence	no convergence

*Elkins et al. (2008) provide a range for U and Th partition coefficients for garnet pyroxenite. For modeled tholeiites, the high end of the range produced no convergence and the low end of the range indicated maximum porosities of 5-7% and solid mantle upwelling velocity of 90-200 cm/yr.